NATIONAL ADVISORY COMMITTEE FOR AERONAUTICS

MEMORANDUM REPORT

for the

Army Air Forces, Air Technical Service Command

WIND-TUNNEL TESTS OF A 1/5-SCALE SEMISPAN MODEL OF THE REPUBLIC XF-12 HORIZONTAL TAIL SURFACE

By H. G. Denaci

Langley Memorial Aeronautical Laboratory
Langley Field, Va.

Suitable for indefinite
(Revised 5/2/45)

MR No. L5D12 [redacted]

NATIONAL ADVISORY COMMITTEE FOR AERONAUTICS

MEMORANDUM REPORT

for the

Army Air Forces, Air Technical Service Command

WIND-TUNNEL TESTS OF A 1/5-SCALE SEMISPAN MODEL OF THE REPUBLIC XF-12 HORIZONTAL TAIL SURFACE

By H. G. Denaci

SUMMARY

Wind-tunnel tests of a 1/5-scale semispan model of the Republic XF-12 horizontal tail surface equipped with an internally balanced elevator were conducted in the 6- by 6-foot test section of the Langley stability tunnel. The tests included measurements of the aerodynamic characteristics of the horizontal tail with and without a beveled trailing edge and also included measurements of the tab characteristics. The variation of the aerodynamic characteristics with boundary-layer conditions and leakage in the internal-balance chambers, measurements of the boundary-layer displacement thickness near the elevator hinge axis, and pressure distributions at the mean geometric chord were also obtained.

The results showed that the hinge-moment characteristics of the elevator were critical to boundary-layer conditions and internal-balance leakage. Increasing the boundary-layer displacement thickness by use of roughness strips reduced the rate of change of elevator hinge moments with tab deflection by about 20 percent. The present horizontal tail appears to be unsatisfactory for longitudinal stability with power on, however, an increase in horizontal-tail lift effectiveness should correct this difficulty. The maneuvering stick force per unit acceleration will be extremely critical to minor variations of the elevator hinge moments if the elevator is linked directly to the stick.

[redacted]TION

At the request of the Army Air Forces, Air Technical Service Command, tests were conducted of a 1/5-scale

semispan model of the Republic XF-12 horizontal tail surface. The XF-12 airplane is a large, fast, high-altitude photographic airplane of conventional design. (See fig. 1.)

These tests, as part of a series of investigations of various components and of a complete model of the XF-12 airplane, were conducted to obtain data useful in the design of the XF-12 horizontal tail. Of general interest, however, is the information obtained on the effects of boundary-layer conditions and leakage on the aerodynamic characteristics of the horizontal tail.

SYMBOLS

The coefficients and symbols used in this report are defined as follows:

C_L lift coefficient (L/qS)

c_l section lift coefficient (l/qc)

C_h hinge-moment coefficient $(H/qb\bar{c}^2)$

C_m pitching-moment coefficient about quarter chord of the mean geometric chord $(M/qc'S)$

C_D drag coefficient (D/qS)

ΔP pressure coefficient across internal balance (pressure below balance minus pressure above balance divided by free-stream dynamic pressure)

P pressure coefficient (local static pressure minus free-stream static pressure divided by free-stream dynamic pressure)

δ^*/c boundary-layer displacement thickness $\left[\int_0^\infty \left(1 - \frac{u}{U}\right) d\left(\frac{y}{c}\right)\right]$

E leakage factor $\left[1 - \frac{p_{(b)} - p_{(c)}}{p_{(a)} - p_{(d)}}\right]$

$p_{(b)}-p_{(c)}$ pressure difference across balance of internal balance

$p_{(a)}-p_{(d)}$ applied pressure difference across vents of internal balance

F overhang factor of complete elevator $\left[\left(\frac{\bar{c}_b}{\bar{c}_e}\right)^2 - \left(\frac{\bar{t}/2}{\bar{c}_e}\right)^2\right]\frac{b_b}{b_e}$

F_1 overhang factor for elevator root chamber $\left[\left(\frac{\bar{c}_{b_1}}{\bar{c}_e}\right)^2 - \left(\frac{\bar{t}_1/2}{\bar{c}_e}\right)^2\right]\frac{b_{b_1}}{b_e}$ (corresponding for F_2 and F_3)

L lift of the semispan model

l section lift

H hinge moment of control surface, positive when tending to rotate the trailing edge down

M pitching moment of semispan model

D drag of semispan model

S area of the semispan model

c local chord

c' mean geometric chord

$\bar{c}$ root mean square chord

b span

$\bar{t}$ root mean square thickness of elevator at elevator hinge axis

u local velocity in boundary layer

U local velocity outside boundary layer

y distance normal to surface of airfoil at which local velocity is measured

q dynamic pressure $\left(\frac{1}{2}\rho V^2\right)$

R Reynolds number $\left(\frac{\rho V c'}{\mu}\right)$

V free-stream velocity

ρ mass density of air

μ viscosity of air

α angle of attack

δ control surace angle relative to surface to which it is hinged, positive when trailing edge is deflected down

ϕ trailing-edge angle

Subscripts

e elevator

t tab

b balance

1 root chamber

2 center chamber

3 tip chamber

Slopes

$C_{L_\alpha} = (\partial C_L/\partial \alpha)_{\delta_e, \delta_t}$

$C_{L_{\delta_e}} = (\partial C_L/\partial \delta_e)_{\alpha, \delta_t}$

$$C_{L_{\delta_t}} = (\partial C_L/\partial \delta_t)_{\alpha, \delta_e}$$

$$C_{h_{e_\alpha}} = (\partial C_{h_e}/\partial \alpha)_{\delta_e, \delta_t}$$

$$C_{h_{e_{\delta_e}}} = (\partial C_{h_e}/\partial \delta_e)_{\alpha, \delta_t}$$

$$C_{h_{e_{\delta_t}}} = (\partial C_{h_e}/\partial \delta_t)_{\alpha, \delta_e}$$

$$C_{h_{t_\alpha}} = (\partial C_{h_t}/\partial \alpha)_{\delta_e, \delta_t}$$

$$C_{h_{t_{\delta_e}}} = (\partial C_{h_t}/\partial \delta_e)_{\alpha, \delta_t}$$

$$C_{h_{t_{\delta_t}}} = (\partial C_{h_t}/\partial \delta_t)_{\alpha, \delta_e}$$

$$(\Delta P)_\alpha = [\partial(\Delta P)/\partial \alpha]_{\delta_e, \delta_t}$$

$$(\Delta P)_{\delta_e} = [\partial(\Delta P)/\partial \delta_e]_{\alpha, \delta_t}$$

$$C_{m_\alpha} = (\partial C_m/\partial \alpha)_{\delta_e, \delta_t}$$

$$C_{m_{\delta_e}} = (\partial C_m/\partial \delta_e)_{\alpha, \delta_t}$$

$$P_\alpha = (\partial P/\partial \alpha)_{\delta_e, \delta_t}$$

$$P_{\delta_e} = (\partial P/\partial \delta_e)_{\alpha, \delta_t}$$

where symbols following parenthesis indicate factors held constant and angles are in degrees.

APPARATUS AND METHODS

Model

The 1/5-scale semispan model of the Republic XF-12 horizontal tail used in these tests was furnished by

the Republic Aviation Corporation. Various photographs of the model are given in figure 2 and a sketch showing the pertinent details of the model is given in figure 3. The tab gap was unsealed for all the tests. The ordinates of the horizontal-tail airfoil contour are presented in table I. Up to the 50-percent station these ordinates are the same as those of the NACA 65_1-012 airfoil; to the rear of this station the ordinates were modified so as to eliminate the cusp. The trailing-edge angle of the elevator was 16° over the inboard, 90 percent of the elevator semispan, and decreased to 13° at the elevator tip. The geometric characteristics of the model are presented in table II.

The internal balance of the elevator was divided into three spanwise chambers at the hinges. (See fig. 2.) The nose and ends of the internal-balance plate in each chamber were sealed to the front of the balance chamber and to the sides of the hinges, respectively, with a continuous strip of flexible material. In order to determine the effect of leakage on the characteristics of the internal-balance elevator, 3/16-inch holes were drilled through the internal-balance overhang at the chordwise location shown in figure 4. The first hole was drilled 1 inch from the root end of the internal-balance overhang and succeeding holes were progressively spaced 1 inch between centers.

A built-up beveled trailing edge was added to the elevator outboard of the tab for the beveled-trailing-edge tests. A sketch of a typical section of the beveled-trailing-edge elevator is given in figure 4. The trailing-edge angle of the beveled elevator was 16° over the tab, 25° outboard of the tab to 90 percent of the elevator span, and decreased to 22° at the elevator tip.

Installation

The semispan model of the XF-12 horizontal tail was mounted horizontally in the 6- by 6-foot test section of the Langley stability tunnel with the root end of the horizontal tail adjacent to one side of the test section which acted as a reflection plane. (See fig. 2.) The model was supported entirely by the balance frame so that all the forces and moments acting on the model could be measured. The portion of the model forward of

54 percent of the root chord protruded through the disc in the tunnel wall to the balance frame; the clearance between the model and the disc was sealed with flexible material. An open gap of 1/16 inch was left between the portion of the model to the rear of 54 percent of the root chord and the tunnel wall. Elevator hinge moments were measured by a spring-torque balance linked to the elevator. Tab hinge moments were measured with a strain gage mounted in the elevator.

Tests

Tests were made of the horizontal-tail model with and without a beveled trailing edge for a range of angles of attack from -13° to 10° and for a range of elevator angles from -24° to 14.5°. These tests included measurements of lift, elevator hinge moment, pitching moment, drag, and pressure difference across the balance for both the smooth model and the model with roughness strips. The designation "smooth model" corresponds to the condition of free transition on the smooth, highly polished model. The "roughness strips" were strips placed on the smooth model at a constant percent of the horizontal-tail chord on both upper and lower surfaces. The strips, whose average height was approximately 0.0007 of the mean geometric chord, were prepared by cementing no. 60 carborundum particles to the back of cellulose tape in a strip 1/4-inch wide.

Measurements of tab hinge moments were made on the horizontal tail without a beveled trailing edge for a range of tab angles from -10° to 25° on both the smooth model and the model with roughness strips at 0.25c. Leakage tests were made on the horizontal tail with roughness strips at 0.25c with one, two, and four inboard holes in each chamber open and with eight holes in the root and center chambers and six holes in the tip chamber open.

Pressure distributions were obtained on the smooth model at the spanwise location of the mean geometric chord. The pressures were measured by a single-tube static mouse attached to the upper surface of the model and moved to various chordwise locations. A previous calibration of the static tube against surface orifices in a model indicates that the pressure coefficients

obtained with the static tube are in the order of 0 to 0.05 more positive than static surface orifices. Velocity profiles were also measured in the boundary layer at 0.65c at the spanwise location of the mean geometric chord. These measurements were made with a mouse consisting of six total-head tubes at various heights above the airfoil surface and one static tube approximately 1/2 inch above the surface. Pressure distributions and boundary-layer measurements for the lower surface of the model were obtained by reversing the angle of attack and elevator angle from the conditions at which measurements were made for the upper surface.

All the tests except those specifically labeled on the figures were made at a dynamic pressure of 64.3 pounds per square foot. The corresponding airspeed under standard sea-level atmospheric conditions is 159 miles per hour and the Reynolds number based on the mean geometric chord is 2.76×10^6. A few force tests were made at a dynamic pressure of 98.3 pounds per square foot and a few boundary-layer tests were inadvertently made at a dynamic pressure of 39.7 pounds per square foot. The corresponding Reynolds numbers are 3.41×10^6 and 2.16×10^6, respectively.

Leakage Determination

The completeness of the internal balance seal in each of the chambers was determined by pressure measurements. A rectangular box was placed over the vent on the upper surface of the model and a pressure difference was applied across the vents of the internal balance as shown schematically in figure 5. If the internal-balance chamber were completely sealed, the leakage factor E would, by definition, equal zero.

Measurements of the leakage factor were made for a series of applied pressure differences from 0 to approximately $\frac{1}{2}q$ for each of the model configurations tested. When determined for comparable seal conditions, the value of E varied in the order of ± 0.02, consequently, all values of E given are average values. The seal in the internal-balance chamber was complete except at the hinges just under the rear end of the cover plates. It is believed that the variations in E were caused by

the seal assuming slightly different positions at the elevator hinge for the various times that E was determined.

Corrections

Lift, elevator hinge moment, pitching moment, drag, pressure difference across the balance, and angle of attack have been corrected for effects of the jet boundaries by the general methods of reference 1. The values used for these tests are:

$$C_L = 0.987C_L'$$

$$C_{h_e} = C_{h_e}' + 0.0060C_L$$

$$C_m = C_m' + 0.0109C_L$$

$$C_D = C_D' + 0.0198C_L^2$$

$$\Delta P_1 = \Delta P_1' - 0.018C_L$$

$$\Delta P_2 = \Delta P_2' - 0.014C_L$$

$$\Delta P_3 = \Delta P_3' - 0.012C_L$$

$$\alpha = \alpha' + 1.35C_L$$

where the primed symbols indicate the uncorrected values. The correction to the tab hinge moments was estimated to be negligible and, consequently, was not applied.

No corrections for jet-boundary effects and interference effects between the mouse tubes and the model have been made to the pressures measured in the pressure distribution and boundary-layer tests. Also, no corrections have been made for the effects of the tunnel-wall boundary layer at the root of the model or for the gap between the rear portion of the root section of the model and the tunnel wall.

RESULTS AND DISCUSSION

Presentation of Data

The results of this investigation are presented in figures 6 to 20. A summary of some of the aerodynamic characteristics of the various modifications tested is given in table III. The slopes were obtained over a small range of angles of attack and elevator and tab angles at approximately $\alpha = \delta_e = \delta_t = 0^\circ$. It will be noticed that several values of the slopes for the horizontal tail are given for identical test conditions. These differences represent the accuracy with which the results could be repeated.

The values of $(\Delta P)_\alpha$, $(\Delta P)_{\delta_e}$, and E given are weighted mean values for the three internal-balance chambers, that is,

$$(\Delta P)_\alpha = \frac{(\Delta P)_{\alpha_1} F_1 + (\Delta P)_{\alpha_2} F_2 + (\Delta P)_{\alpha_3} F_3}{F}$$

and correspondingly for $(\Delta P)_{\delta_e}$ and E.

Although pressure differences across the balance were measured for all three internal-balance chambers, only the results for the root chamber are presented in the plots. Pressure differences for the center and tip chambers, when neither the horizontal tail or the elevator are stalled, may be estimated from the following empirical relations.

$$\Delta P_2 = 0.97 \Delta P_1$$

$$\Delta P_3 = 0.78 \Delta P_1$$

These relations were obtained from a comparison of the pressures in the three chambers for various angles of attack and deflections. These relations apply to the model both with and without the roughness strips or bevel and are approximately correct for the tests with additional leakage. Beyond the stall no definite

relation was found for the pressure differences in the three chambers.

Boundary-Layer Measurements

It was considered desirable to simulate on the model the calculated boundary-layer displacement thickness just ahead of the elevator hinge axis so that the aerodynamic characteristics of the model may more nearly represent the characteristics of the horizontal tail in flight. The Reynolds number of the horizontal tail of the XF-12 airplane flying at 400 miles per hour at 40,000 feet altitude (the design cruising condition) is approximately 10^7. Because the airplane horizontal tail may under some conditions of flight be operating in the slipstream and because the surface roughness of a combat airplane may be relatively large, the transition in flight may occur near the nose of the horizontal tail. Unpublished theoretical calculations of the boundary-layer displacement thickness δ^*/c at 0.65c on the NACA 65_1-012 airfoil with transition at the leading edge and at $R = 10^7$ gave a value of δ^*/c of 0.00157 at $c_l = 0$. The boundary-layer displacement thickness may be considered as the thickness to be added to the airfoil contour to obtain the effective airfoil contour.

The velocity profiles through the boundary layer, measured on the horizontal-tail model, are shown in figure 6. Values of δ^*/c are given in figure 7. A comparison of the measured and theoretical values of δ^*/c indicates that with strips on the model at 0.25c, the theoretical boundary-layer conditions on the airplane were approximately simulated at $\alpha = \delta_e = 0^\circ$. As the lift coefficient is varied by changing the angle of attack, δ^*/c increases more rapidly on the upper surface and decreases more rapidly on the lower surface than was calculated theoretically for the NACA 65_1-012 airfoil with transition at the leading edge and with $R = 10^7$. It is apparent, therefore, that in order to simulate the theoretical boundary-layer conditions for other angles of attack and deflections, the strips must be relocated on the model for every conditions. Since the roughness strips were not relocated on the model for every condition, the effect of the roughness strips determined in this investigation does not simulate the effect of movement of transition on the actual horizontal tail.

The location of transition on the smooth model was not determined. (See fig. 7.)

Aerodynamic Characteristics of the Horizontal Tail

The coefficients of lift, elevator hinge moment, pitching moment, drag, and pressure difference across the balance of the horizontal tail are given in figure 8 for the smooth model and in figure 9 for the model with roughness strips at 0.25c. The leakage factor E changed during these tests; however, a study of the test conditions, the model, and the data indicate that the tests of the smooth model were made at $E = 0.03$ and the tests with the roughness strips at 0.25c were made between $E = 0.03$ and $E = 0.12$.

Because the angles of attack for which the data were obtained in figures 8 and 9 were not close enough to define completely the curves of C_{h_e} against α and because of the differences in the leakage, additional tests were made of the horizontal tail. The results of these tests are presented in figure 10. For the smooth model the curves of C_{h_e} against α are approximately linear between -2° to 2° and at these limits abrupt changes occurred. Although it is not apparent in the drag of the complete model, this range corresponds approximately to the low-drag range of the airfoil. It is believed that, as the angle of attack increases beyond the low-drag range, transition on the upper surface abruptly moves forward with a corresponding large increase in δ^*/c over the rear portion of the airfoil; whereas, on the lower surface transition gradually moves rearward with a corresponding decrease in δ^*/c. Such changes in δ^*/c produce a change in effective camber which results in positive hinge-moment increments for positive angles of attack. It is also expected that the larger the trailing-edge angle the larger the change in hinge moments. By limiting the movement of transition (placing roughness strips near the airfoil leading edge), it is believed that the changes in δ^*/c with angle of attack become more gradual. Figure 10 shows that the roughness strips reduced or eliminated the abrupt changes in the hinge-moment curves with an attendant positive increase in $C_{h_{e_\alpha}}$ over the small range of angles of attack.

The effects of boundary-layer conditions on the variations of C_L and ΔP with α were so small as to be within the accuracies of the tests. The variations of $C_{h_{e_{\delta_e}}}$, $C_{L_{\delta_e}}$, and $(\Delta P)_{\delta_e}$ with boundary-layer conditions are, however, of relatively large magnitude. (See fig. 10 and table III). These variations are such that $C_{h_{e_{\delta_e}}}$ becomes more positive with roughness and $C_{L_{\delta_e}}$ and $(\Delta P)_{\delta_e}$ become more negative.

The roughness strips at 0.25c on the model were intended to duplicate the flow conditions on the actual horizontal tail at small deflections only. At large elevator deflections, it is believed that the smooth model more nearly represents the conditions of the actual horizontal tail because the roughness strips hastened rather than delayed the separation over the elevator.

Aerodynamic Characteristics of the Horizontal Tail with a Beveled Trailing Edge

A beveled trailing edge was added to the elevator outboard of the tab to provide data on this means of increasing the balance of hinge moments. The bevel was only added outboard of the tab so as not to decrease the tab effectiveness. The incremental effects of the tab, therefore, should be directly applicable to the beveled elevator.

The results of the tests of the beveled-tailing-edge elevator on the smooth model and the model with roughness strips at 0.25c are given in figures 11 and 12, respectively. A comparison of the effects of roughness is given in figure 13. In figure 12, the points at $\alpha \approx 0^\circ$ for various elevator deflections (the tests were run at constant α in the tunnel against δ_e; the variation of α is caused by the jet-boundary correction) were ignored in the fairing because of the unusual character of the results for that run. The run was not checked but all other tests indicate the fairing to be more reasonable than the actual points.

The effects of boundary-layer conditions on the aerodynamic characteristics of the beveled-trailing-edge elevator (except for the one unusual run) were

similar to but, as to be expected, of greater magnitude than those described for the elevator without the bevel. The extremely critical nature of model surface conditions on the variation of C_{h_e} with α is illustrated in figure 13. Results are shown for a test of the model without strips but with a considerable number of small particles (insects present in the tunnel at night) on and near the airfoil leading edge. This case gave almost the same results as roughness strips at 0.05c.

Tab Characteristics

The results of the tests of the tab on the elevator without a beveled trailing edge are given in figure 14 for the smooth model and in figure 15 for the model with roughness strips at 0.25c. The tab tested is capable of trimming to zero the elevator hinge moments of only -10° to 10° elevator deflections at all angles of attack for tab deflections of 25° to -25°. At positive angles of attack, however, the tab is capable of trimming -15° to -20° elevator deflections, depending on the boundary-layer conditions. It appears, nevertheless, that for the airplane in the landing or take-off conditions a tab of greater span or chord may be necessary when large up-elevator deflections are required. The tab effectiveness $C_{h_{e_{\delta_t}}}$ can also be increased approximately 25 percent by sealing the tab gap. (See reference 2.) The roughness strips reduced the value of $C_{h_{e_{\delta_t}}}$ by about 20 percent.

Effect of Leakage

A practical installation of an internal balance will, of necessity, have some leakage for draining condensation. In order to determine the effects of leakage, tests of the horizontal tail were conducted with various numbers of holes through the internal-balance plate simulating leak area. (See fig. 16.) The effect of the holes on the leakage factor of the individual chambers is given in figure 17(a). The variation of the aerodynamic characteristics with the weighted mean leakage factor are given in figures 17(b) to 17(d). Since it is apparent that the characteristics of an internal balance are critically dependent on leakage, it is suggested that manufacturers and maintenance

crews give consideration to the pressure-measurement method of checking the completeness of the seal on all internally balanced control surfaces.

It is usually assumed that the balancing action or increment of hinge moment produced by the overhang in an internal balance is directly proportional to the product one-half the overhang factor times the pressure difference across the balance. The data of figure 17, however, show increments of $C_{h_{e_\alpha}}$ and $C_{h_{e_{\delta_e}}}$ with leakage which are less negative than those calculated from the balancing pressure $(\Delta P)_\alpha$ and $(\Delta P)_{\delta_e}$. Although leakage may cause negative increments in $C_{h_{e_\alpha}}$ and $C_{h_{e_{\delta_e}}}$ of a plain control surface when the pressure recovery over the rear of the airfoil is unusually adverse or when the trailing-edge angle is small, the data of reference 3 show that the increments of $C_{h_{e_\alpha}}$ and $C_{h_{e_{\delta_e}}}$ due to leakage will become increasingly positive as the trailing-edge angle is increased.

The effect of leakage on C_{L_α} was so small as to be within the accuracy of the tests. For the range of leakage tested, however, leakage caused approximately a 9-percent reduction in $C_{L_{\delta_e}}$.

Pressure Distributions

The results of pressure-distribution tests on the smooth model of the horizontal tail without the bevel for several angles of attack and elevator deflections are given in figure 18. Because of the differences in the readings of the static mouse tube and a surface orifice, it is advisable not to use the pressure distributions where a high degree of accuracy is required. The variation of the pressure coefficients with angle of attack and elevator deflection, as determined from the data of figures 18(a), 18(b), and 18(c), is given in figure 19.

Some Estimated Characteristics of the XF-12 Airplane

In the absence of tests of a complete model of the XF-12 airplane, an estimate was made in the Stability and Control Section of the Langley Flight Research Division of the neutral point of the airplane with stick fixed and propellers windmilling. The estimated neutral-point location was 37.8 percent of the mean aerodynamic chord. The airplane pitching moments caused by the horizontal tail were based on the assumptions that the variation of horizontal-tail lift coefficient with tail angle of attack is 0.070 per degree, the variation of wing-lift coefficient with angle of attack is 0.084 per degree, the variation of downwash angle with angle of attack is 0.36, and the dynamic-pressure ratio at the tail is 0.9. When the analysis is modified to take into account the slope of the horizontal-tail lift-coefficient curve obtained in the present investigation, the revised estimated neutral point is 36.0 percent of the mean aerodynamic chord. Since the most rearward center-of-gravity position is 35 percent of the mean aerodynamic chord, the airplane will be longitudinally stable (stick fixed and propellers windmilling) on the basis of these estimates. Assuming, however, that the effects of power shift the neutral point 6 percent of the mean aerodynamic chord further forward, it is estimated that a 14-percent increase in the horizontal-tail lift effectiveness will be required to make the airplane neutrally stable with stick fixed at the most rearward center-of-gravity location.

Estimates of the stick force per unit normal acceleration are given in figure 20. These estimates were made by the methods given in reference 4 using the slopes of table III. It was assumed that the ratio of stick movement to elevator deflection with tab fixed is 1.80 feet per radian and that the ratio of stick movement to tab deflection with elevator fixed is -1.20 feet per radian. It is apparent from figure 20 that none of the model configurations tested are capable of producing satisfactory variations of stick force per unit acceleration over the center-of-gravity range. Furthermore, it is apparent that if the airplane is to be controlled with the elevator linked directly to the stick, the stick force per unit acceleration will be extremely critical to minor variations of the elevator hinge-moment characteristics. The maneuvering forces with a servotab in conjunction with the smooth horizontal

tail (ϕ = 25° outboard of tab) indicate forces too small to be considered satisfactory. The characteristics of a spring tab approach those of a servotab at high speed with the exception that the stick forces are increased by the amount required to deflect the spring. The analysis of reference 4 indicates that if the elevator hinge moments are adjusted to give values of $C_{h_{e_\alpha}}$ and $C_{h_{e_{\delta_e}}}$ in the order of 0.0000 and 0.0030 per degree, respectively, satisfactory variations of stick force per unit acceleration can be obtained over the speed and center-of-gravity range by a proper selection of spring and tab gearing.

Comments on Layout of Internal-Balance Chambers

It can be seen in figure 3 that the tip chamber covers approximately 0.15 of the total internal-balance span. The ratio of the overhang factor of the tip chamber to the total overhang factor F_3/F, however, is only 0.08. This ratio, when multiplied by the relation between the pressure difference in the tip and root chambers or tip and center chamber, indicates that the aerodynamic balance produced by the tip chamber is only 6 percent of the total for the three chambers. Since the installation and maintenance of the internal balance for three chambers requires more work than for two chambers, it appears that it may, from a practical viewpoint, be desirable to replace the internal balance in the tip chamber by a round nose, using a wiper seal to retain the lift effectiveness. Part of the loss due to eliminating the overhang in the tip chamber could be recovered by extending the span of the center chamber.

CONCLUSIONS

The results of the tests of the 1/5-scale semispan model of the XF-12 horizontal tail indicate the following general conclusions:

1. The hinge-moment characteristics of the elevator vary considerably with boundary-layer conditions and the magnitude of the variation increases with trailing-edge angle.

2. The balance characteristics of the internal-balance elevator are critically dependent on leakage.

3. Increasing the boundary-layer displacement thickness by use of roughness strips on the tail surfaces reduced the rate of change of elevator hinge moments with tab deflection by about 20 percent.

4. Although the tip chamber of the internal balance contributes only approximately 6 percent of the total aerodynamic balance for the three chambers, it covers about 15 percent of the total span and adds to the amount of work required to install and maintain the internal balance.

5. Estimates indicate that the present horizontal tail will be satisfactory for longitudinal stability with stick fixed and propellers windmilling. The effects of power will probably make the airplane longitudinally unstable at the most rearward center-of-gravity location, however, an increase in the horizontal-tail lift effectiveness should correct this difficulty.

6. The maneuvering stick force per unit acceleration will be extremely critical to minor variations of the elevator hinge moments if the elevator is linked directly to the stick.

Langley Memorial Aeronautical Laboratory
National Advisory Committee for Aeronautics
Langley Field, Va.

Herbert G. Denaci

Herbert G. Denaci
Aeronautical Engineer

Approved:

Hartley A. Soulé

Hartley A. Soulé
Chief of Stability Research Division

ES

REFERENCES

1. Swanson, Robert S., and Toll, Thomas A.: Jet-Boundary Corrections for Reflection-Plane Models in Rectangular Wind Tunnels. NACA ARR No. 3E22, 1943.

2. Lowry, John G., Maloney, James A., and Garner, I. Elizabeth: Wind-Tunnel Investigation of Shielded Horn Balances and Tabs on a 0.7-Scale Model of XF6F Vertical Tail Surface. NACA ACR No. 4C11, 1944.

3. Hoggard, H. Page, Jr., and Bulloch, Marjorie E.: Wind-Tunnel Investigation of Control-Surface Characteristics. XVI - Pressure Distribution over an NACA 0009 Airfoil with 0.30-Airfoil-Chord Beveled-Trailing-Edge Flaps. NACA ARR No. L4D03, 1944.

4. Phillips, William H.: Application of Spring Tabs to Elevator Controls. NACA ARR No. L4H28, 1944.

TABLE I

ORDINATES OF THE XF-12 HORIZONTAL-TAIL AIRFOIL SECTION

[Stations and ordinates are in percent of airfoil chord]

Station	Ordinate
0	0
.50	±.923
.75	±1.109
1.25	±1.387
2.50	±1.875
5.00	±2.606
7.50	±3.172
10.00	±3.647
15.00	±4.402
20.00	±4.975
25.00	±5.407
30.00	±5.716
35.00	±5.912
40.00	±5.997
45.00	±5.949
50.00	±5.757
55.00	±5.449
60.00	±5.041
65.00	±4.535
70.00	±3.970
75.00	±3.367
80.00	±2.715
85.00	±2.056
90.00	±1.395
95.00	±.707
100.00	0
L. E. Radius: 1.000	

NATIONAL ADVISORY
COMMITTEE FOR AERONAUTICS

TABLE II

GEOMETRIC CONSTANTS OF THE 1/5-SCALE SEMISPAN MODEL

OF THE XF-12 HORIZONTAL TAIL SURFACE

Area of semispan model, S, square feet	7.82
Span of semispan model, b, feet	4.42
Mean geometric chord of model, c', feet	1.854
Span of semispan elevator, b_e, feet	3.75
Span of internal balance of semispan elevator, b_b, feet	3.53
Root mean square chord of elevator, $\bar{c}_e$, feet	0.571
Root mean square chord of internal balance to center of seal, $\bar{c}_b$, feet	0.234
Root mean square thickness of elevator at elevator hinge axis, $\bar{t}$, feet	0.148
Area of internal balance to the center of the flexible seal divided by the area of the elevator, S_b/S_e	0.38
Span of semispan tab, b_t, feet	1.55
Root mean square chord of tab, $\bar{c}_t$, feet	0.132
Aspect ratio of complete horizontal tail	5.00
Taper ratio of horizontal tail	0.50
Overhang factor of complete internal balance, F	0.141
Overhang factor of root chamber, F_1	0.078
Overhang factor of center chamber, F_2	0.052
Overhang factor of tip chamber, F_3	0.011

NATIONAL ADVISORY
COMMITTEE FOR AERONAUTICS

TABLE III

SUMMARY OF AERODYNAMIC CHARACTERISTICS OF THE XP-12 HORIZONTAL-TAIL MODEL

[All values were measured over a small range at angles of attack and deflections at approximately $\alpha = \delta_e = \delta_t = 0^\circ$]

Designation	Boundary-layer condition	Leakage factor E	C_{L_α}	$C_{L_{\delta_e}}$	$C_{L_{\delta_t}}$	$\frac{C_{L_{\delta_e}}}{C_{L_\alpha}}$	$\frac{C_{L_{\delta_t}}}{C_{L_\alpha}}$	$C_{h_{e_\alpha}}$	$C_{h_{e_{\delta_e}}}$	$C_{h_{e_{\delta_t}}}$	$C_{h_{t_\alpha}}$	$C_{h_{t_{\delta_e}}}$	$C_{h_{t_{\delta_t}}}$	$(\Delta P)_\alpha$	$(\Delta P)_{\delta_e}$	C_{m_α}	$C_{m_{\delta_e}}$	$C_{D_{min}}$
Horizontal-tail model ($\phi = 16^\circ$), (figs. 8 to 10)	Smooth model	0.03	0.067	0.039	-----	0.58	----	[a]-0.0001	-0.0027	-------	------	-------	-------	0.015	0.078	0.0025	-0.0079	0.0075
	Roughness strips at 0.25c	From 0.03 to .12	.067	.035	-----	.52	----	[a]-.0008	-.0018	-------	------	-------	-------	.015	.064	.0022	-.0068	.0100
	Smooth model	.05	.067	.040	-----	.60	----	-.0013	-.0031	-------	------	-------	-------	.017	.082	------	-------	------
	Roughness strips at 0.25c	.05	.067	.034	-----	.51	----	-.0011	-.0015	-------	------	-------	-------	.017	.071	------	-------	------
	---do --- ($R = 3.41 \times 10^6$)	.05	.067	.034	-----	.51	----	-.0007	-.0014	-------	------	-------	-------	.017	.073	------	-------	------
	Roughness strips at 0.05c	.05	.067	.032	-----	.48	----	-.0002	-.0012	-------	------	-------	-------	.017	.069	------	-------	------
Horizontal-tail model with a beveled trailing edge ($\phi = 25^\circ$ outboard of tab) (figs. 11 to 13)	Smooth model	0.05	0.067	0.040	-----	0.60	----	0.0001	-0.0026	-------	------	-------	-------	0.015	0.077	0.0028	-0.0080	0.0075
	Roughness strips at 0.25c	.05	.067	.038	-----	.57	----	.0003	.0005	-------	------	-------	-------	.016	.075	.0030	-.0070	.0103
	Roughness strips at 0.05c	.05	.067	-----	-----	----	----	.0015	-------	-------	------	-------	-------	.016	-----	------	-------	------
	"Particals" at leading edge	.05	.067	-----	-----	----	----	.0015	-------	-------	------	-------	-------	.015	-----	------	-------	------
Horizontal-tail model ($\phi = 16^\circ$), tab tests, (figs. 14 and 15)	Smooth model	0.05	0.067	0.038	0.005	0.57	0.07	[a]0.0001	-0.0034	-0.0058	0.0009	-0.0008	-0.0063	-----	-----	------	-------	------
	Roughness strips at 0.25c	.05	.067	.034	.004	.51	.06	[a]-.0002	-.0020	-.0048	.0003	-.0004	-.0054	-----	-----	------	-------	------
Horizontal-tail model ($\phi = 16^\circ$), leakage tests (fig. 16)	Roughness strips at 0.25c	0.05	0.067	0.035	-----	0.52	----	-0.0008	-0.0015	-------	------	-------	-------	0.017	0.066	------	-------	------
	---do ---	.08	.067	.035	-----	.52	----	-.0008	-.0017	-------	------	-------	-------	.015	.058	------	-------	------
	--- do ---	.10	.067	.034	-----	.51	----	-.0009	-.0022	-------	------	-------	-------	.013	.048	------	-------	------
	--- do ---	.16	.067	.033	-----	.49	----	-.0011	-.0025	-------	------	-------	-------	.011	.044	------	-------	------
	--- do ---	.28	.067	.032	-----	.48	----	-.0013	-.0029	-------	------	-------	-------	.008	.034	------	-------	------

[a] Insufficient points to accurately define slope.

NATIONAL ADVISORY
COMMITTEE FOR AERONAUTICS

MR No. L5D12

MR No. L5D12

FIGURE LEGENDS

Figure 1.- Three-view drawing of Republic XF-12 airplane.

Figure 2.- The 1/5-scale semispan model of the XF-12 horizontal tail mounted in the 6- by 6-foot test section of the Langley stability tunnel.

(a) Front view showing static mouse mounted at the mean geometric chord.

Figure 2.- Continued.

(b) Rear view.

Figure 2.- Concluded.

(c) Rear view showing built-up beveled trailing edge outboard of tab and roughness strips at 0.25c.

Figure 3.- Details of the 1/5-scale model of XF-12 horizontal tail surface.

Figure 4.- Typical section of XF-12 elevator outboard of tab.

Figure 5.- Schematic sketch of the method used to determine the leakage factor.

Figure 6.- Velocity profiles measured at 0.65c at the spanwise location of the mean geometric chord of the XF-12 horizontal tail model ($\Lambda = 16^\circ$). $\delta_e = \delta_t = 0^\circ$.

(a) $\alpha = 0^\circ$, $C_L = 0$.

Figure 6.- Concluded.

(b) Roughness strips at 0.25c, $R = 2.76 \times 10^6$.

Figure 7.- Measured values of δ^*/c at 0.65c at the spanwise location of the mean geometric chord of the XF-12 horizontal tail model, and unpublished theoretically computed values of δ^*/c for the NACA 65_1-012 airfoil at $R = 10^7$. $\delta_e = \delta_t = 0^\circ$.

FIGURE LEGENDS - Continued

Figure 8.- Aerodynamic characteristics of the XF-12 horizontal tail model ($\phi = 16^\circ$). Smooth model, $E = 0.03$, $\delta_t = 0^\circ$.

(a) Lift coefficient.

Figure 8.- Continued.

(b) Elevator hinge-moment coefficient.

Figure 8.- Continued.

(c) Pitching-moment coefficient.

Figure 8.- Continued.

(d) Drag coefficient.

Figure 8.- Concluded.

(e) Pressure coefficient across the balance.

Figure 9.- Aerodynamic characteristics of the XF-12 horizontal tail model ($\phi = 16^\circ$). Roughness strips at 0.25c, $E = 0.03$ to 0.12, $\delta_t = 0^\circ$.

(a) Lift coefficient.

Figure 9.- Continued.

(b) Elevator hinge-moment coefficient.

Figure 9.- Continued.

(c) Pitching-moment coefficient.

Figure 9.- Continued.

(d) Drag coefficient.

Figure 9.- Concluded.

(e) Pressure coefficient across the balance.

FIGURE LEGENDS - Continued

Figure 10.- Aerodynamic characteristics of the XF-12 horizontal tail model ($\phi = 16^\circ$) for various configurations. $E = 0.05$, $\delta_t = 0^\circ$.

(a) $\delta_e = 0^\circ$.

Figure 10.- Concluded.

(b) α, deg $= 0 + 1.35C_L$.

Figure 11.- Aerodynamic characteristics of the XF-12 horizontal tail model with a beveled trailing edge ($\phi = 25^\circ$ outboard of tab). Smooth model, $E = 0.05$, $\delta_t = 0^\circ$.

(a) Lift coefficient.

Figure 11.- Continued.

(b) Elevator hinge-moment coefficient.

Figure 11.- Continued.

(c) Pitching-moment coefficient.

Figure 11.- Continued.

(d) Drag coefficient.

Figure 11.- Concluded.

(e) Pressure coefficient across the balance.

Figure 12.- Aerodynamic characteristics of the XF-12 horizontal tail model with a beveled trailing edge ($\phi = 25^\circ$ outboard of tab). Roughness strips at 0.25c, $E = 0.05$, $\delta_t = 0^\circ$.

(a) Lift coefficient.

Figure 12.- Continued.

(b) Elevator hinge-moment coefficient.

Figure 12.- Continued.

(c) Pitching-moment coefficient.

FIGURE LEGENDS - Continued

Figure 12.- Continued.

(d) Drag coefficient.

Figure 12.- Concluded.

(e) Pressure coefficient across the balance.

Figure 13.- Aerodynamic characteristics of the XF-12 horizontal tail model with a beveled trailing edge ($\phi = 25^\circ$ outboard of tab) for various configurations. $E = 0.05$, $\delta_t = 0^\circ$.

Figure 14.- Tab tests of the XF-12 horizontal tail model ($\phi = 16^\circ$). Smooth model, $E = 0.05$.

(a) α, deg = $10 + 1.35C_L$.

Figure 14.- Continued.

(b) α, deg = $5 + 1.35C_L$.

Figure 14.- Continued.

(c) α, deg = $0 + 1.35C_L$.

Figure 14.- Continued.

(d) α, deg = $-5 + 1.35C_L$.

Figure 14.- Concluded.

(e) α, deg = $-10 + 1.35C_L$.

Figure 15.- Tab tests of the XF-12 horizontal tail model. Roughness strips at 0.25c, $E = 0.05$.

(a) α, deg = $10 + 1.35C_L$.

Figure 15.- Continued.

(b) α, deg = $5 + 1.35C_L$.

FIGURE LEGENDS - Continued

Figure 15.- Continued.

(c) α, deg = 0 + 1.35C_L.

Figure 15.- Continued.

(d) α, deg = -5 + 1.35C_L.

Figure 15.- Concluded.

(e) α, deg = -10 + 1.35C_L.

Figure 16.- Leakage tests of the XF-12 horizontal tail model (ϕ = 16°). Roughness strips at 0.25c. δ_t = 0°.

(a) δ_e = 0°.

Figure 16.- Concluded.

(b) α, deg = 0 + 1.35C_L.

Figure 17.- Summary of the effects of leakage on the characteristics of the XF-12 horizontal tail model (ϕ = 16°). Roughness strips at 0.25c, δ_t = 0°.

Figure 18.- Pressure distributions at the mean geometric chord of the XF-12 horizontal tail model (ϕ = 16°). Smooth model, δ_t = 0°.

(a) α = 0°, δ_e = 0°, C_L = 0, c_l = 0.

Figure 18.- Continued.

(b) α = 5.0°, δ_e = 0°, C_L = 0.33, c_l = 0.35.

Figure 18.- Continued.

(c) α = 0°, δ_e = 5.0°, C_L = 0.19, c_l = 0.22.

Figure 18.- Continued.

(d) α = 4.5°, δ_e = 5.0°, C_L = 0.47, c_l = 0.52.

FIGURE LEGENDS - Concluded

Figure 18.- Concluded.

(e) $\alpha = -1.0^\circ$, $\delta_e = -2.5^\circ$, $C_L = -0.16$, $c_l = -0.20$.

Figure 19.- P_α and P_{δ_e} at the mean geometric chord of the XF-12 horizontal tail model ($\phi = 16^\circ$). Smooth model, $\delta_t = 0^\circ$.

Figure 20.- Estimated maneuvering force characteristics of the XF-12 airplane in pull-ups with aerodynamic balance and with a servo tab on the elevator.

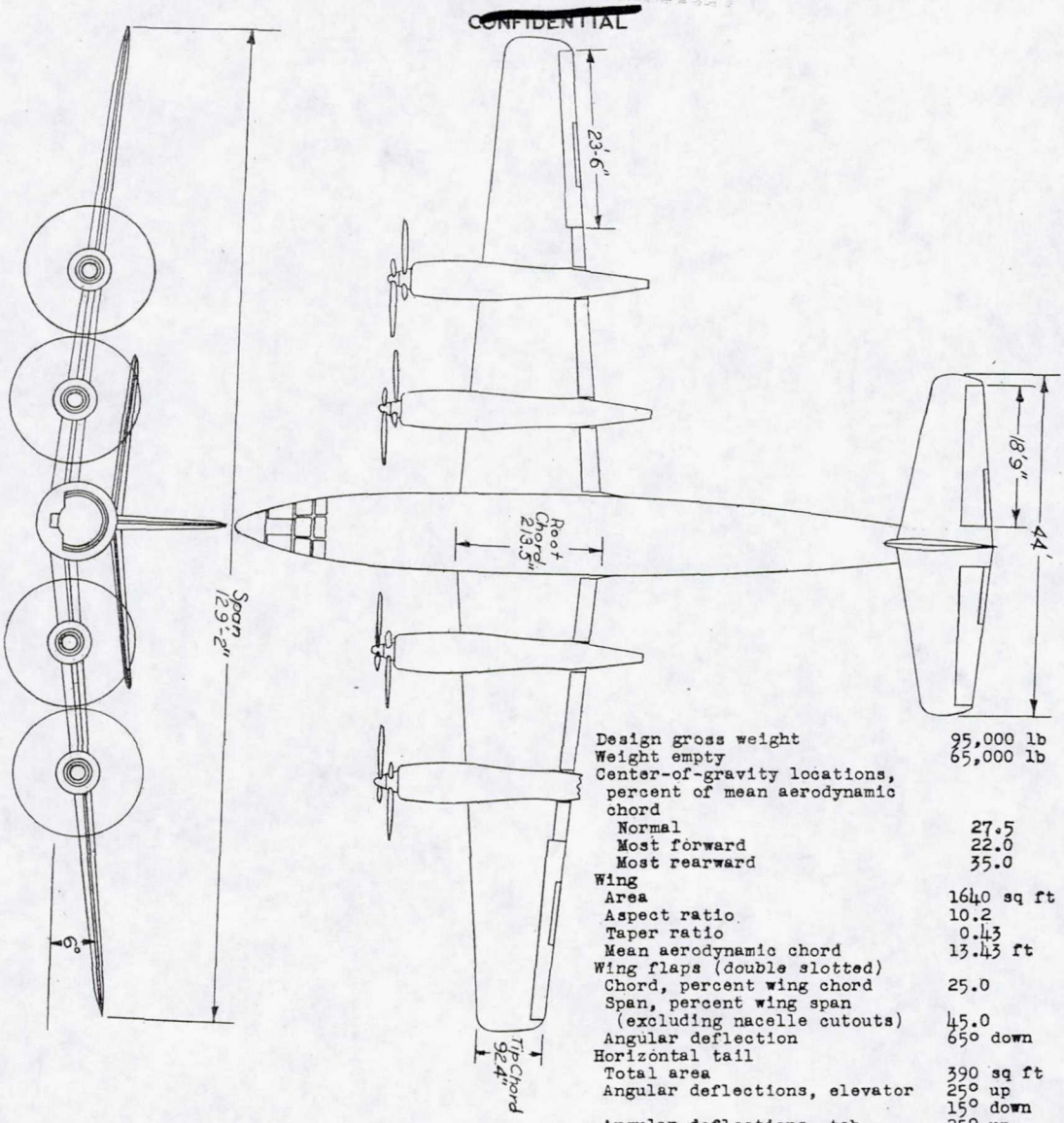

Design gross weight	95,000 lb
Weight empty	65,000 lb
Center-of-gravity locations, percent of mean aerodynamic chord	
Normal	27.5
Most forward	22.0
Most rearward	35.0
Wing	
Area	1640 sq ft
Aspect ratio	10.2
Taper ratio	0.43
Mean aerodynamic chord	13.43 ft
Wing flaps (double slotted)	
Chord, percent wing chord	25.0
Span, percent wing span (excluding nacelle cutouts)	45.0
Angular deflection	65° down
Horizontal tail	
Total area	390 sq ft
Angular deflections, elevator	25° up 15° down
Angular deflections, tab	25° up 25° down
Tail length, 0.25 mean aerodynamic chord to aerodynamic center of tail	52.7 ft

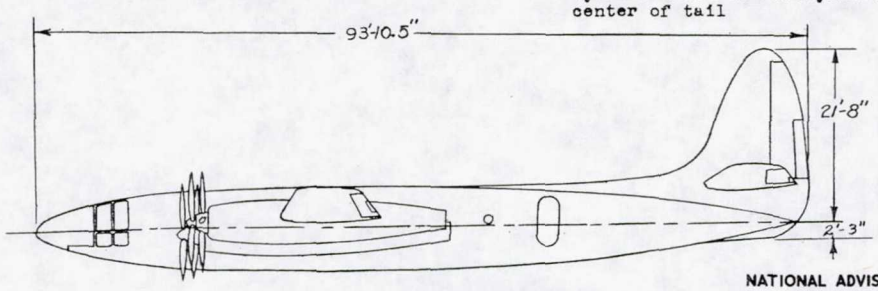

NATIONAL ADVISORY
COMMITTEE FOR AERONAUTICS

Figure 1 .- Three-view drawing of Republic XF-12 airplane.

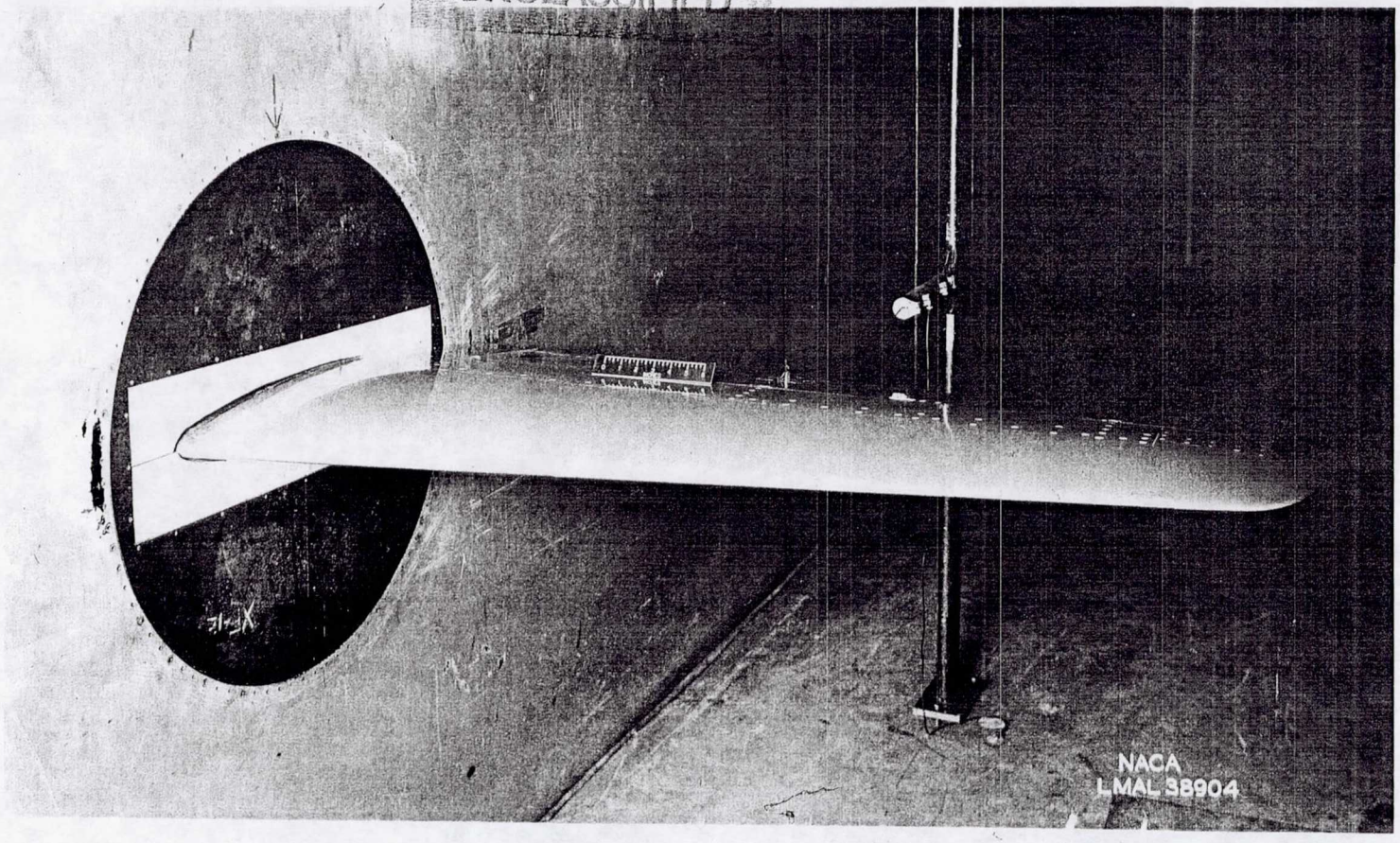

(a) Front view showing static mouse mounted at the mean geometric chord.

Figure 2.- The 1/5-scale semispan model of the XF-12 horizontal tail mounted in the 6- by 6-foot test section of the Langley stability tunnel.

NATIONAL ADVISORY COMMITTEE FOR AERONAUTICS
LANGLEY MEMORIAL AERONAUTICAL LABORATORY - LANGLEY FIELD, VA.

MR No. L5D12

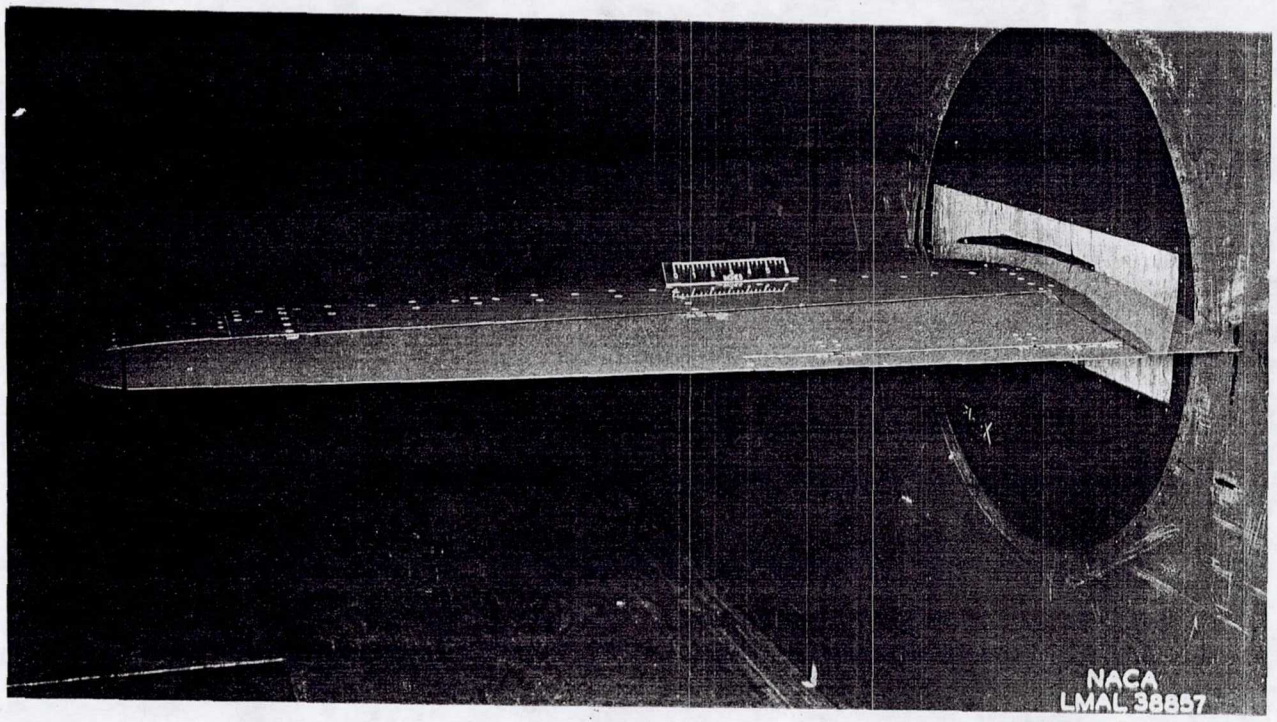

(b) Rear view.

Figure 2.- Continued.

NATIONAL ADVISORY COMMITTEE FOR AERONAUTICS
LANGLEY MEMORIAL AERONAUTICAL LABORATORY - LANGLEY FIELD, VA.

MR No. L5D12

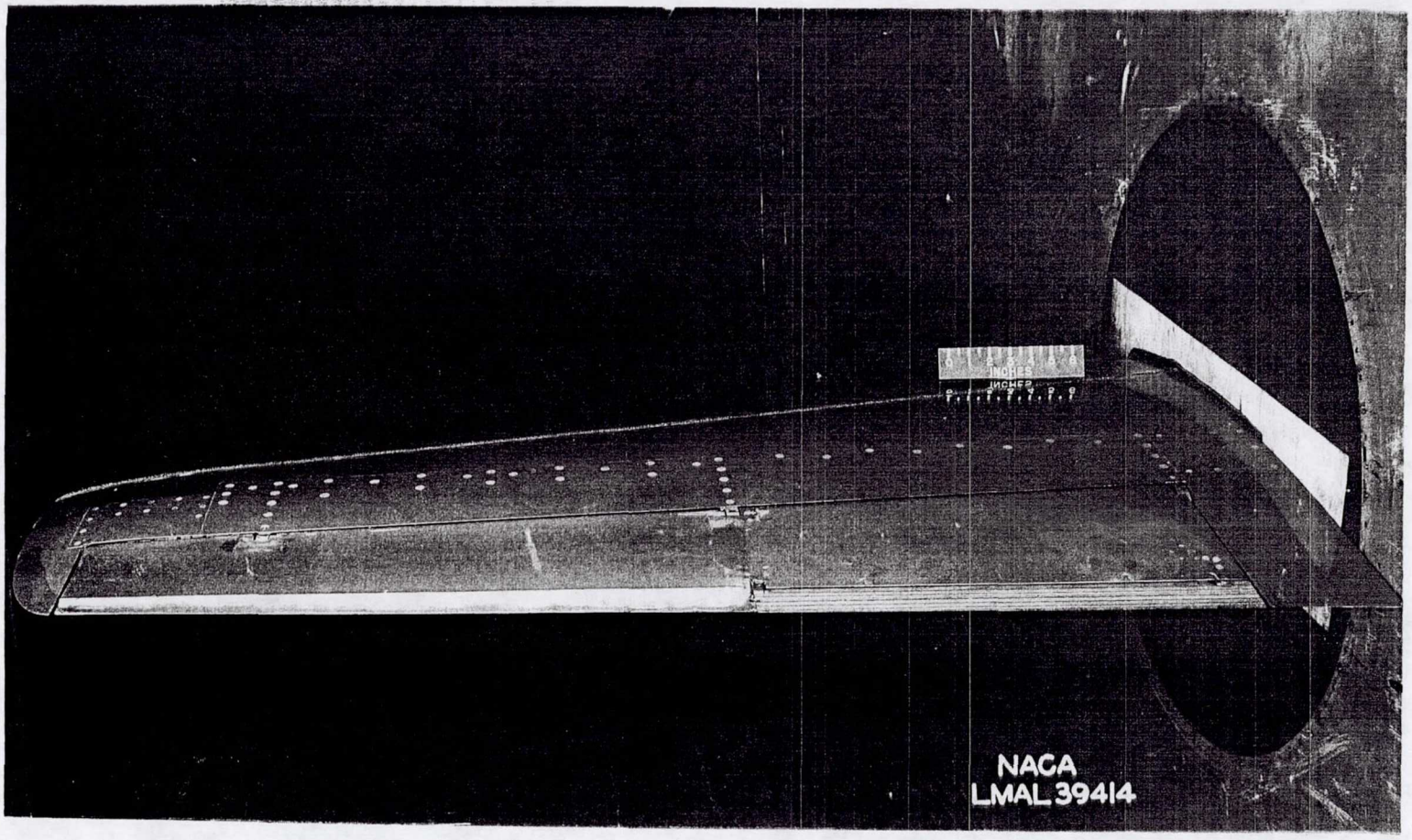

(c) Rear view showing built-up beveled trailing edge outboard of tab and roughness strips at 0.25c.

Figure 2.- Concluded.

NATIONAL ADVISORY COMMITTEE FOR AERONAUTICS
LANGLEY MEMORIAL AERONAUTICAL LABORATORY - LANGLEY FIELD, VA.

NR No. L5D12

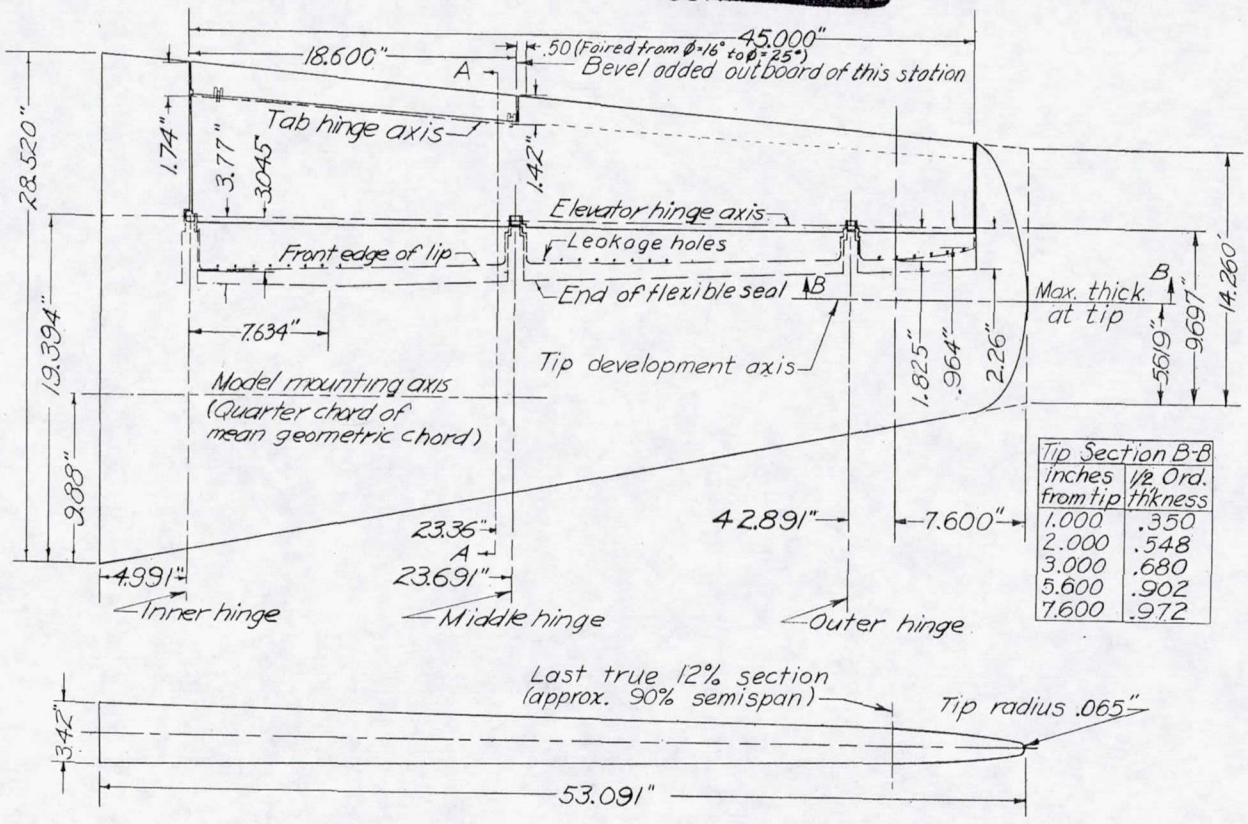

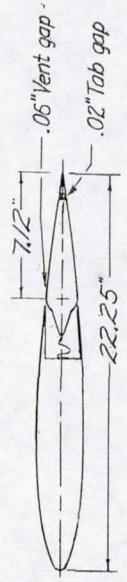

Section A-A
Mean geometric chord

Tip Section B-B	
inches from tip	½ Ord. thickness
1.000	.350
2.000	.548
3.000	.680
5.600	.902
7.600	.972

Tip Development			
Leading edge		Trailing edge	
inches from tip	Chordwise Ordinate	inches from tip	Chordwise Ordinate
.200	2.148	.200	3.079
.400	2.990	.400	4.291
1.000	4.494	.600	5.174
1.400	5.124	1.000	6.453
2.000	5.764	1.600	7.698
2.400	6.036	2.000	8.235
2.800	6.204	2.400	8.588
3.000	6.252	2.800	8.778
		3.000	8.814

Figure 3. — Details of the 1/5-scale model of XF-12 horizontal tail surface

NATIONAL ADVISORY
COMMITTEE FOR AERONAUTICS

MR No. L5D12

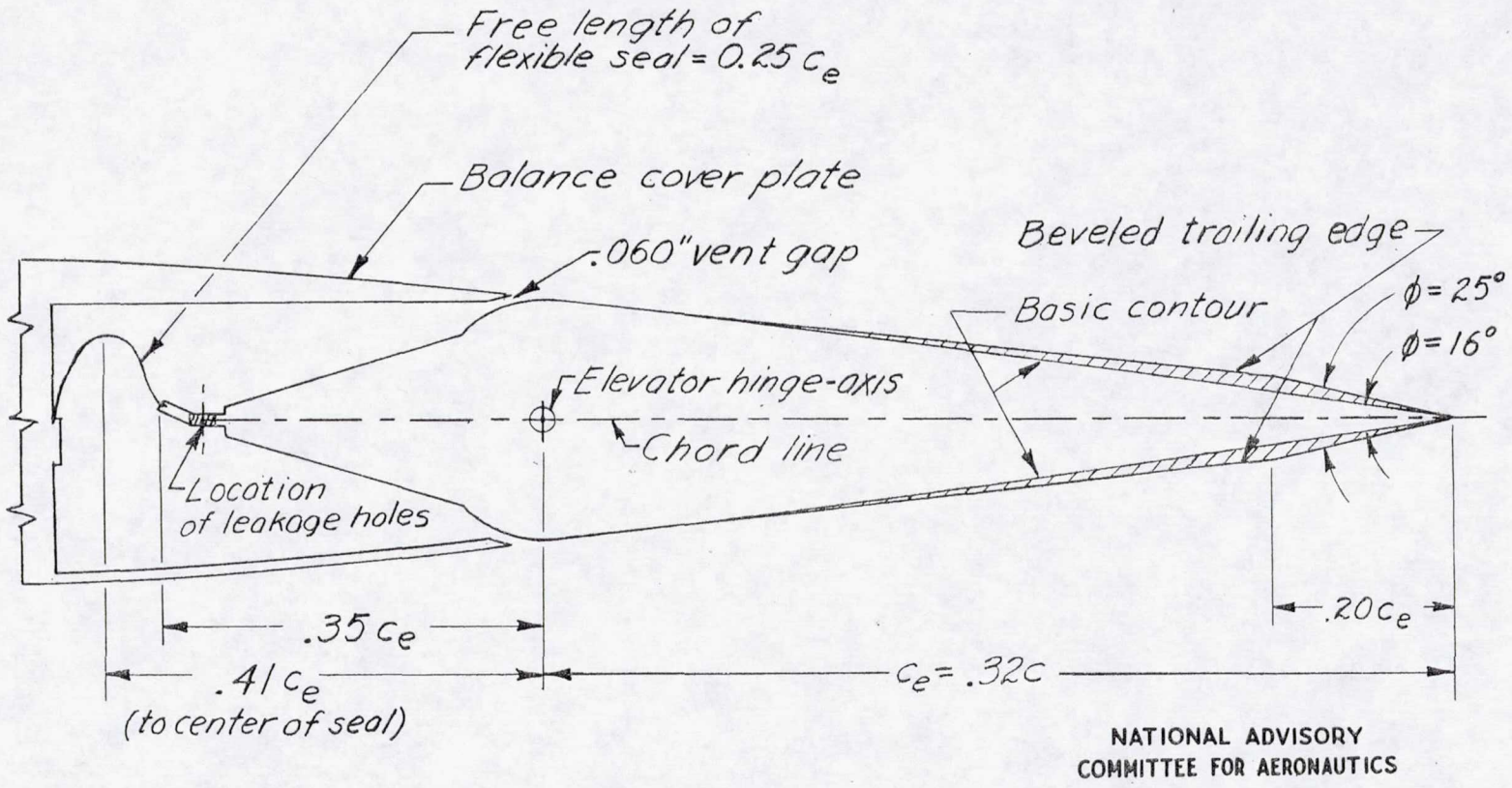

Figure 4. —Typical section of XF-12 elevator outboard of tab.

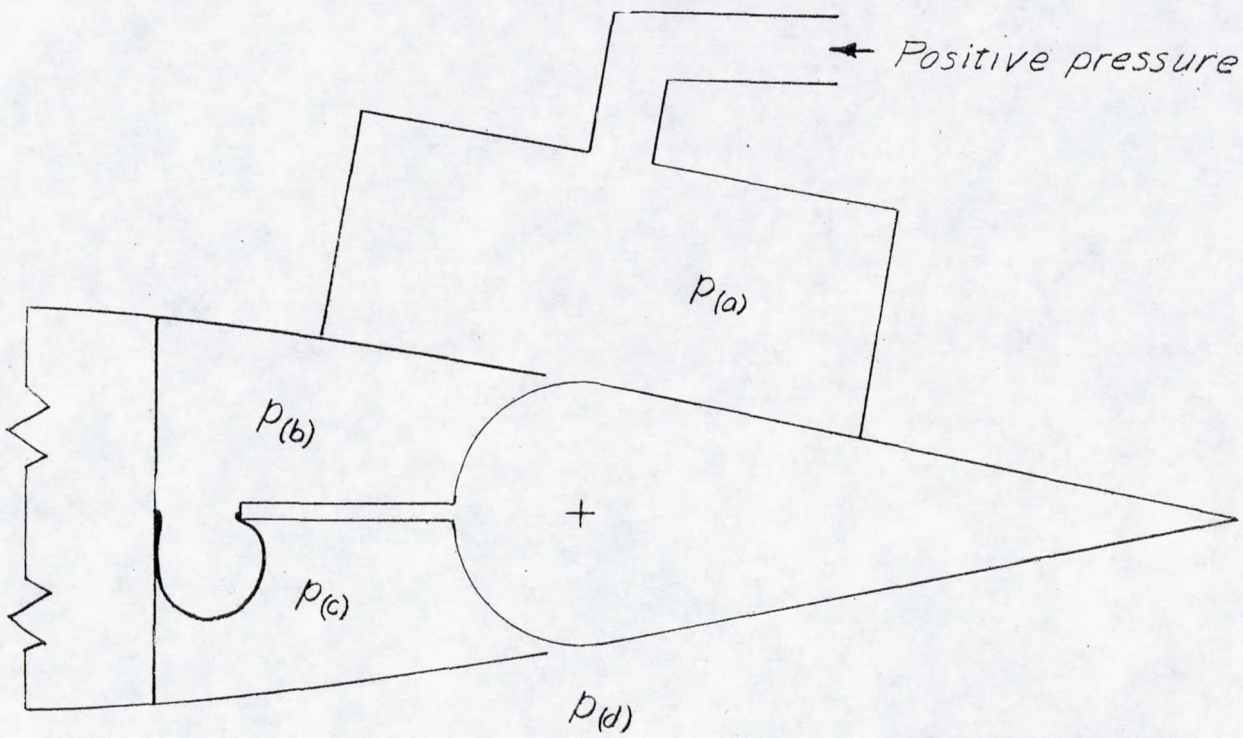

NATIONAL ADVISORY
COMMITTEE FOR AERONAUTICS

$$\text{Leakage factor, } E = \left[1 - \frac{p_{(b)} - p_{(c)}}{p_{(a)} - p_{(d)}}\right]$$

Figure 5.— Schematic sketch of the method used to determine the leakage factor.

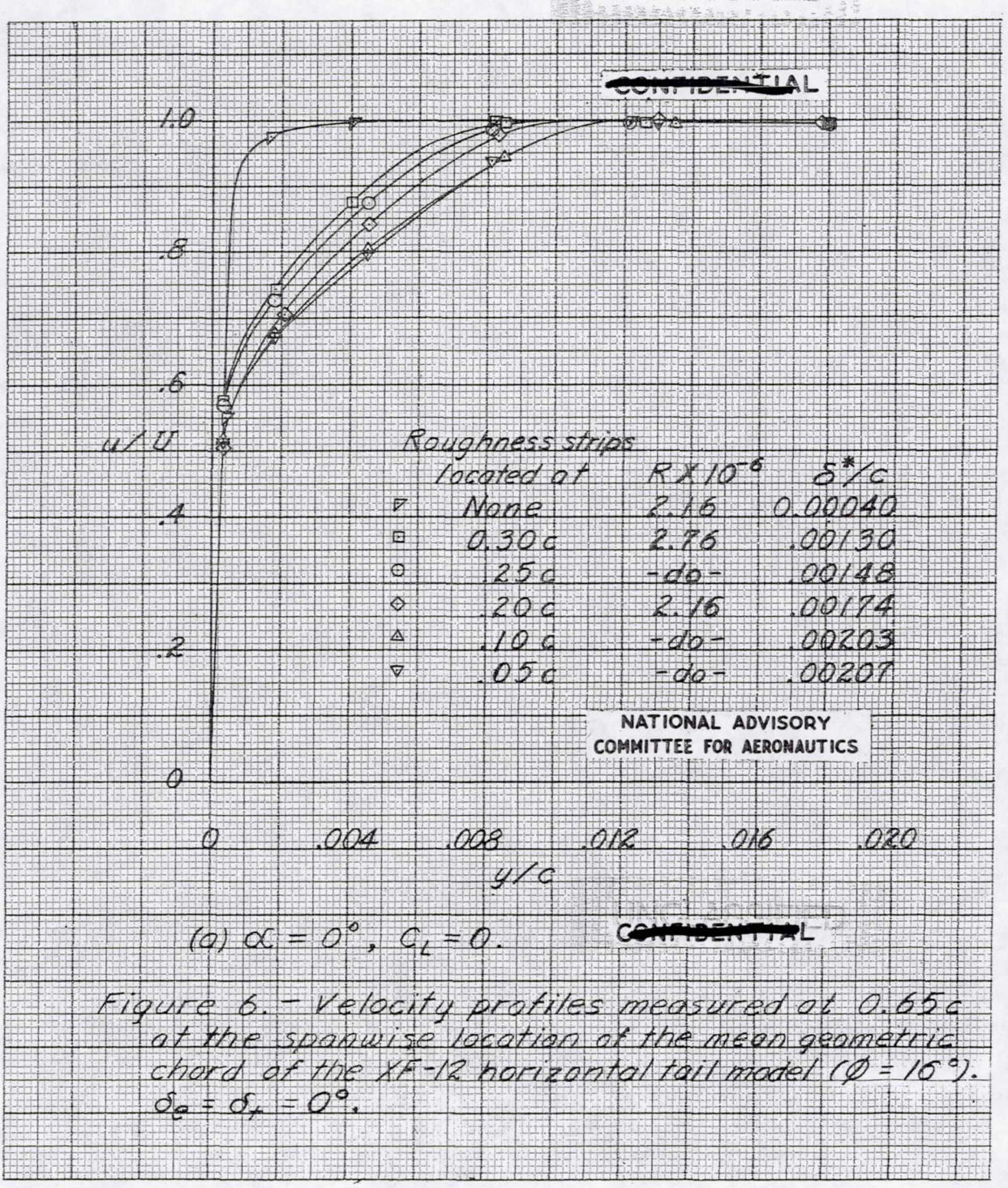

(a) $\alpha = 0°$, $C_L = 0$.

Figure 6. – Velocity profiles measured at 0.65c at the spanwise location of the mean geometric chord of the XF-12 horizontal tail model ($\Phi = 16°$). $\delta_e = \delta_t = 0°$.

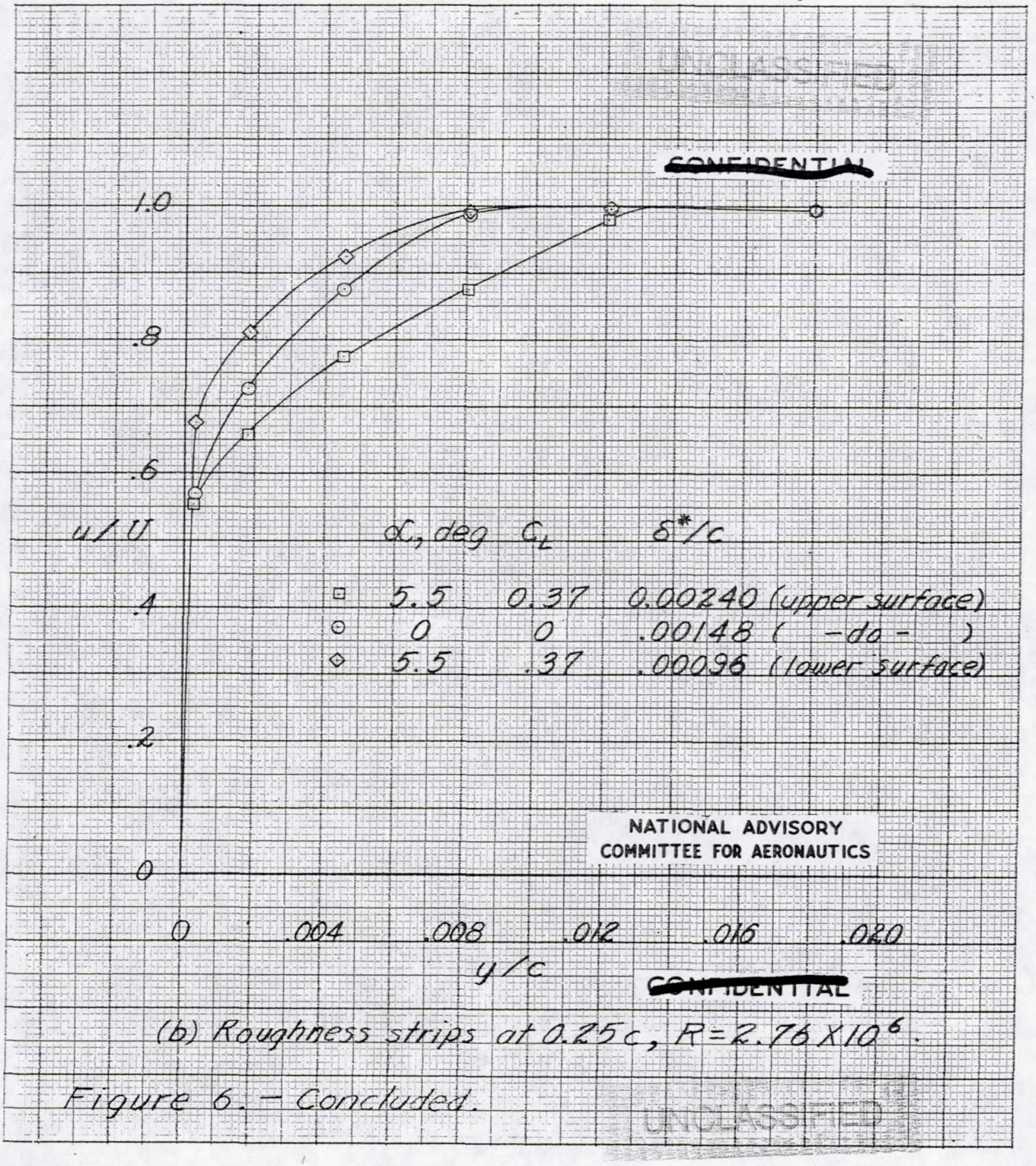

(b) Roughness strips at 0.25c, $R = 2.76 \times 10^6$.

Figure 6. – Concluded.

"Page missing from available version"

"Page missing from available version"

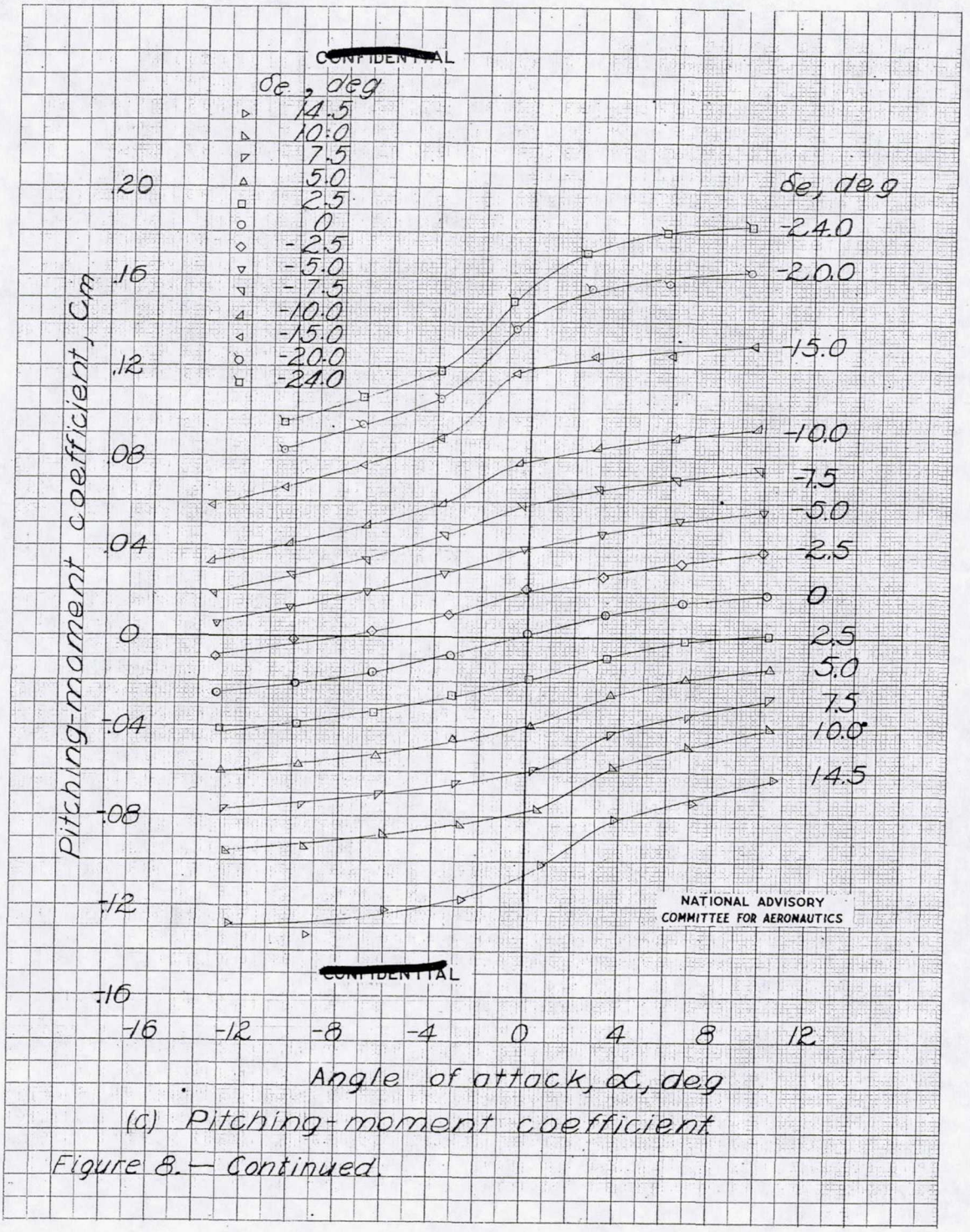

(c) Pitching-moment coefficient

Figure 8.— Continued.

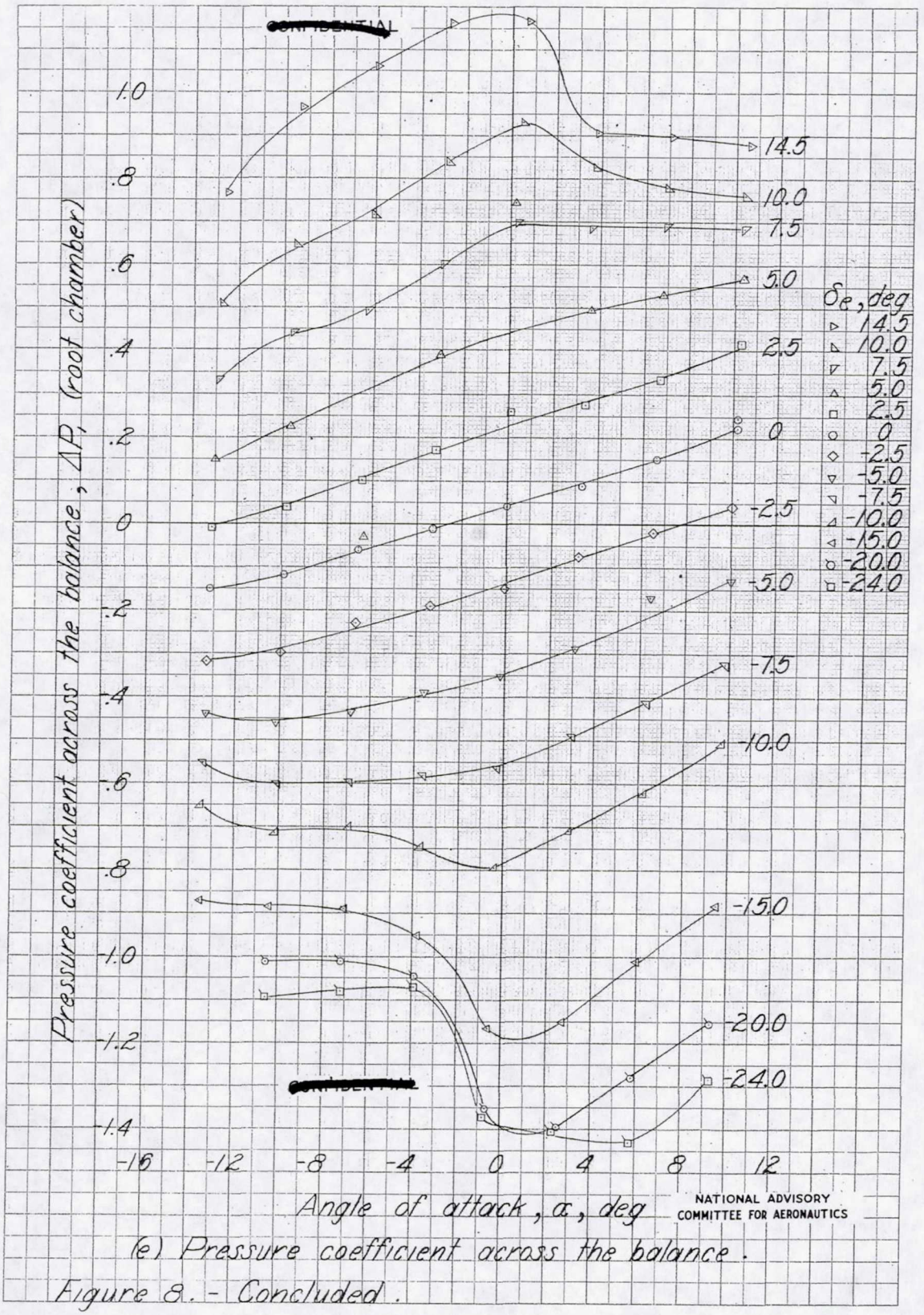

(e) Pressure coefficient across the balance.

Figure 8.- Concluded.

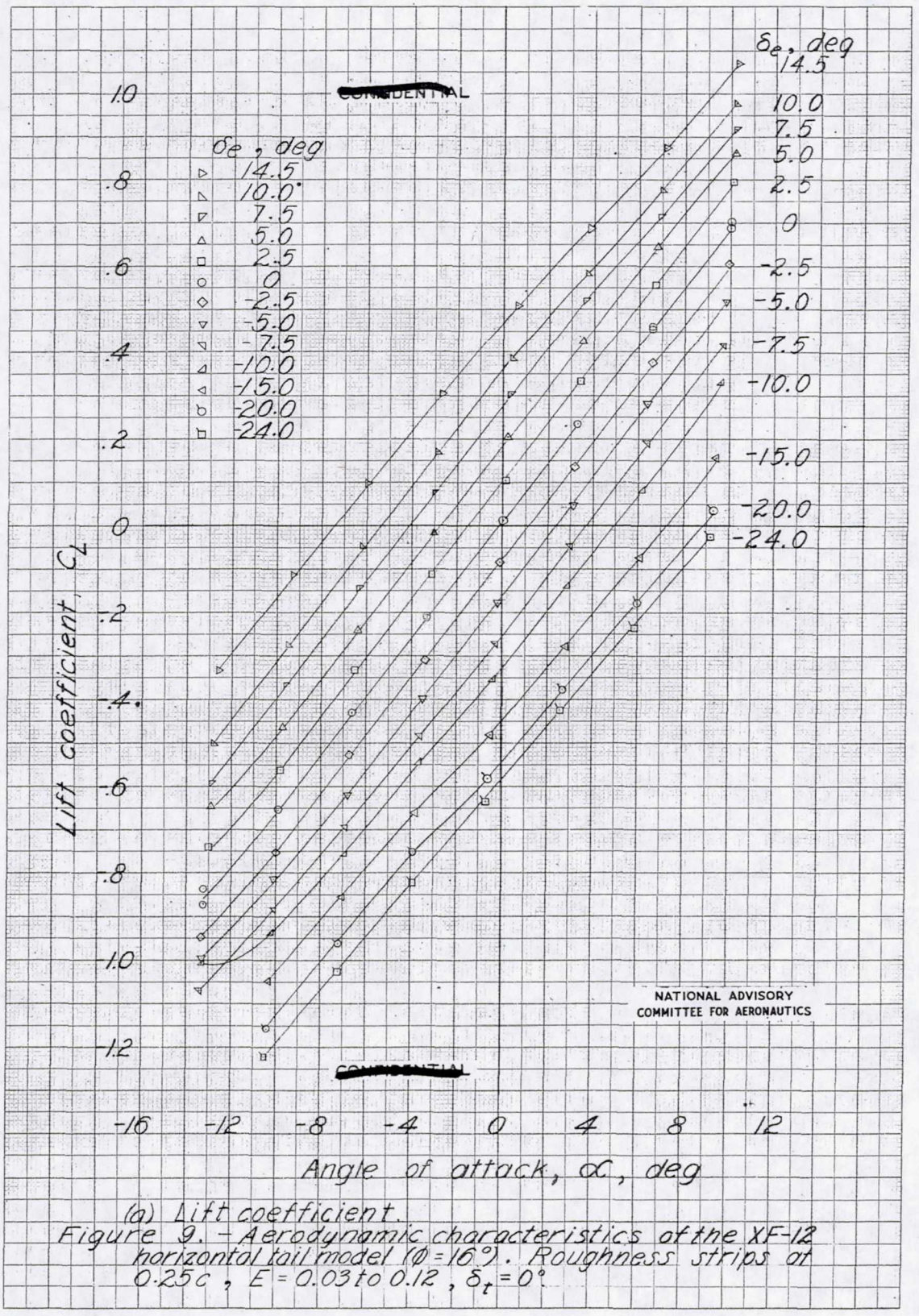

(a) Lift coefficient.

Figure 9. - Aerodynamic characteristics of the XF-12 horizontal tail model ($\Phi = 16°$). Roughness strips at 0.25c, E = 0.03 to 0.12, $\delta_t = 0°$.

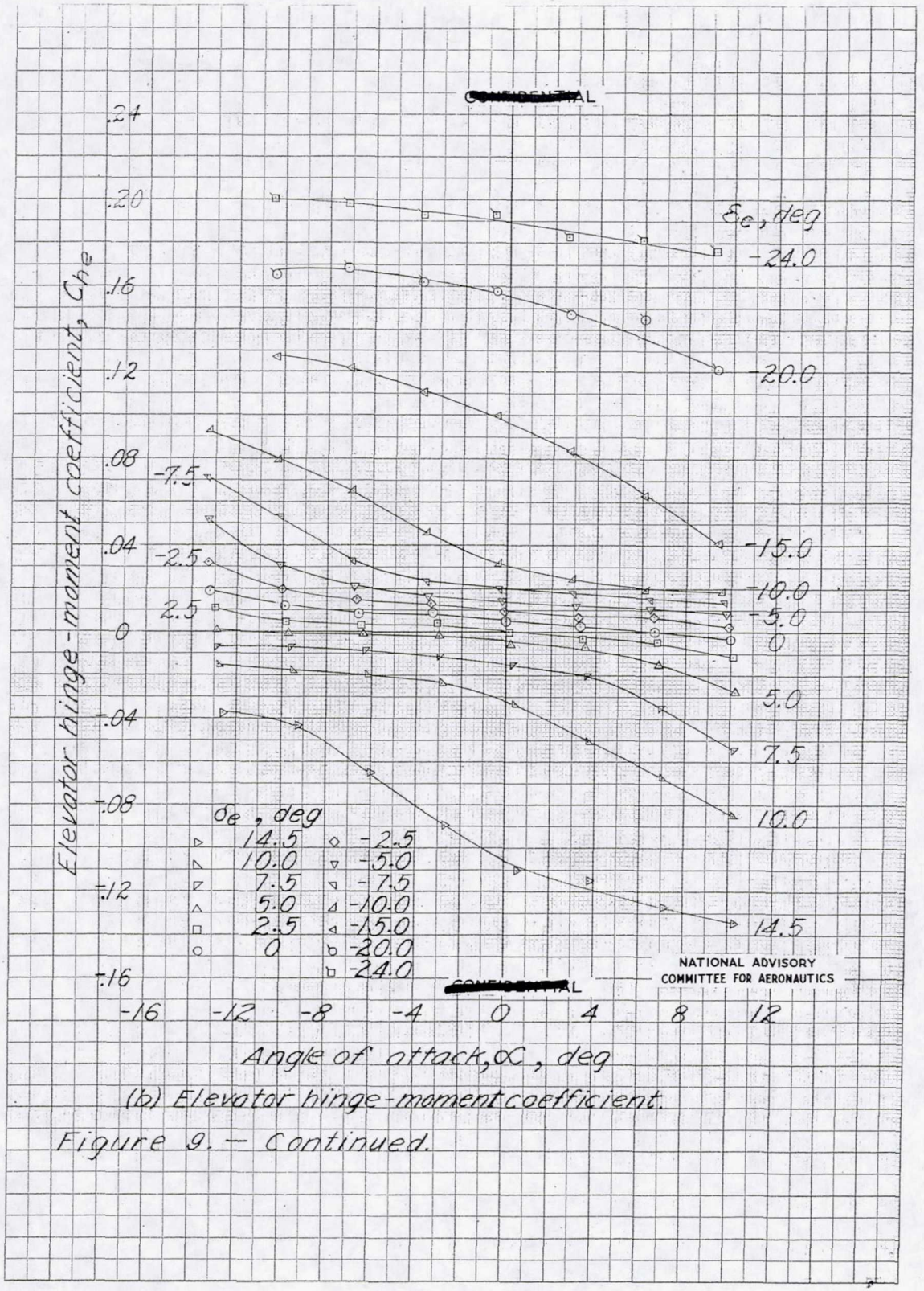

(b) Elevator hinge-moment coefficient.

Figure 9. — Continued.

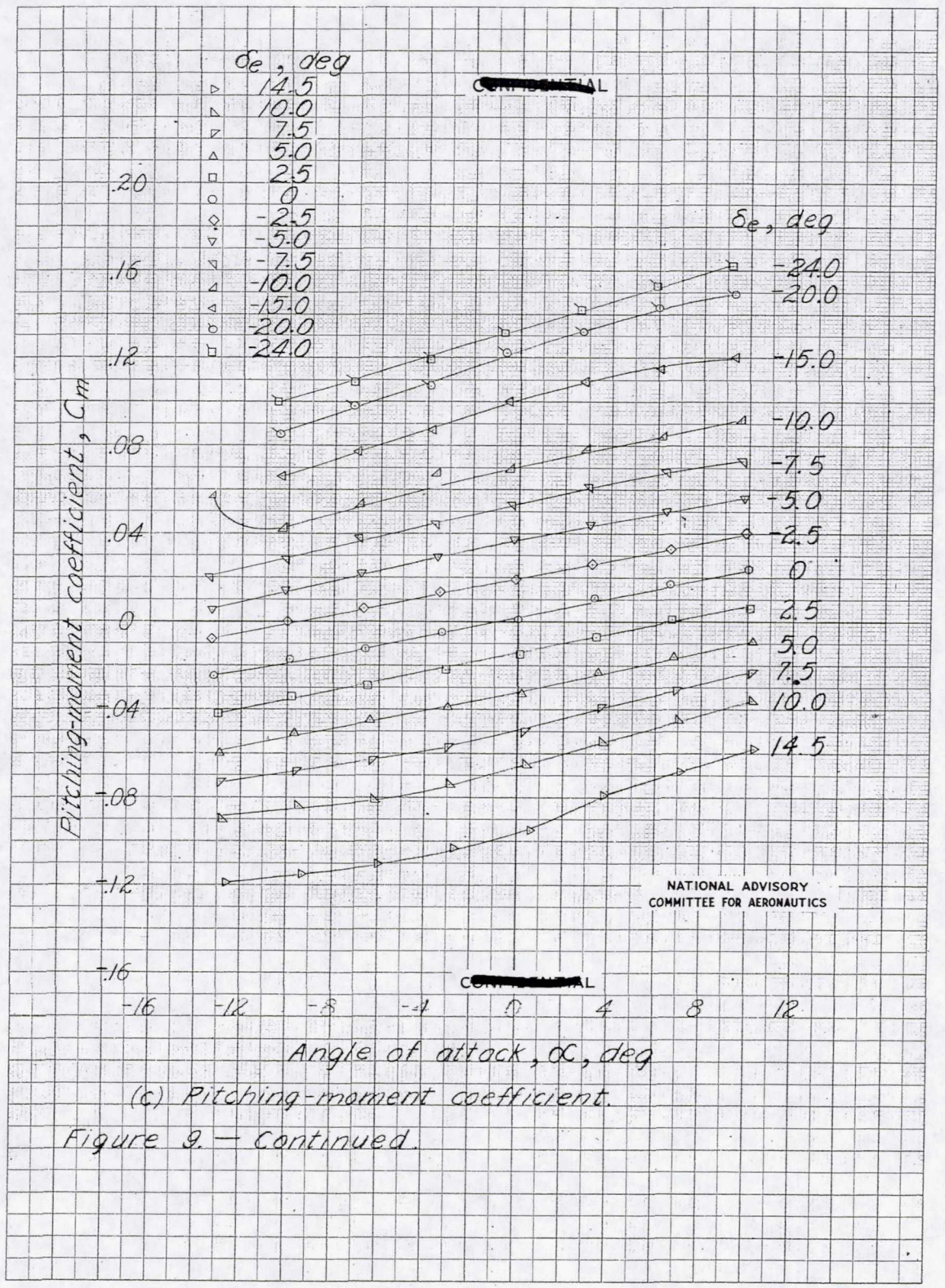

(c) Pitching-moment coefficient.

Figure 9. — Continued.

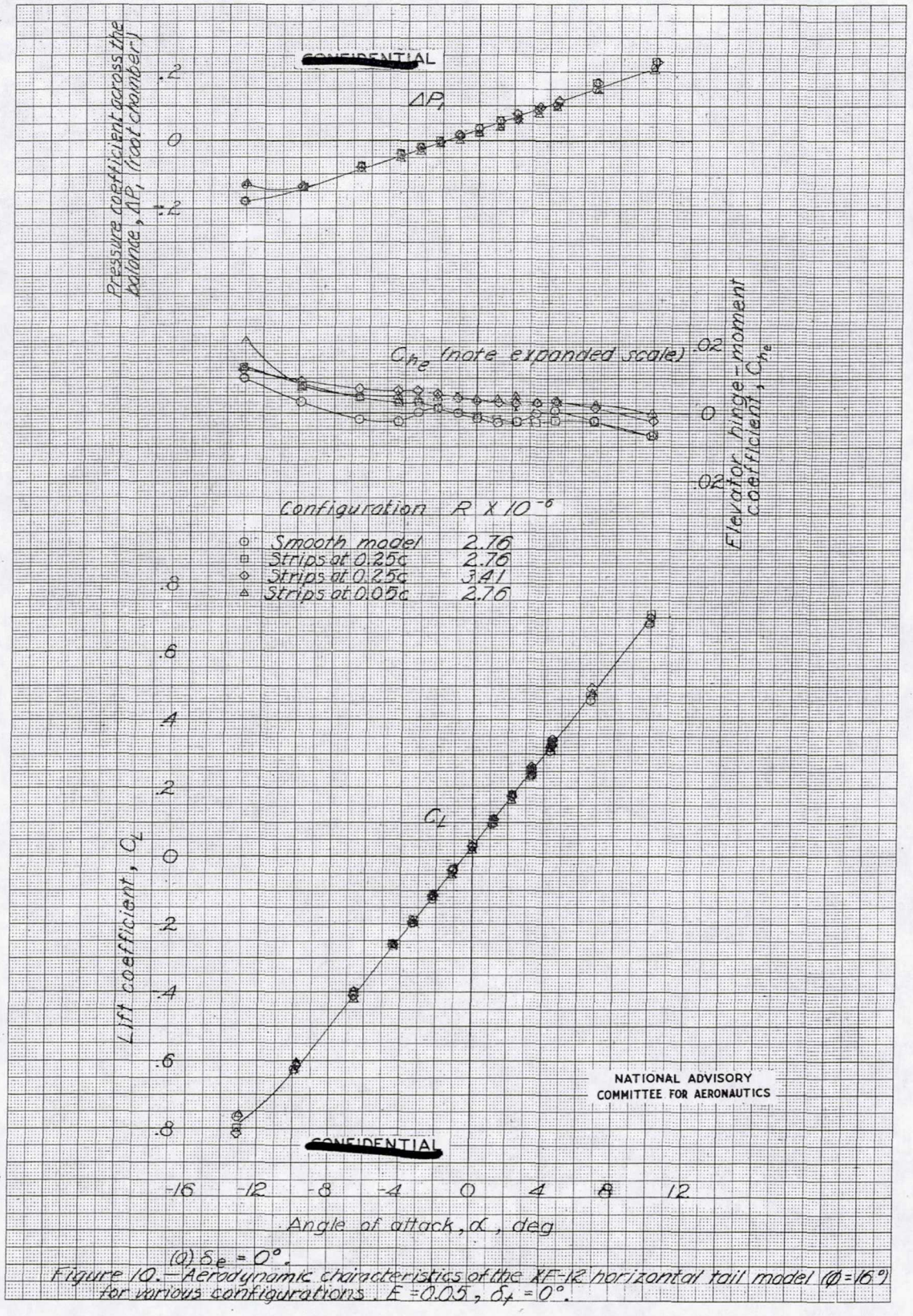

(a) $\delta_e = 0°$.

Figure 10.- Aerodynamic characteristics of the XF-12 horizontal tail model ($\Phi = 16°$) for various configurations. $E = 0.05$, $\delta_t = 0°$.

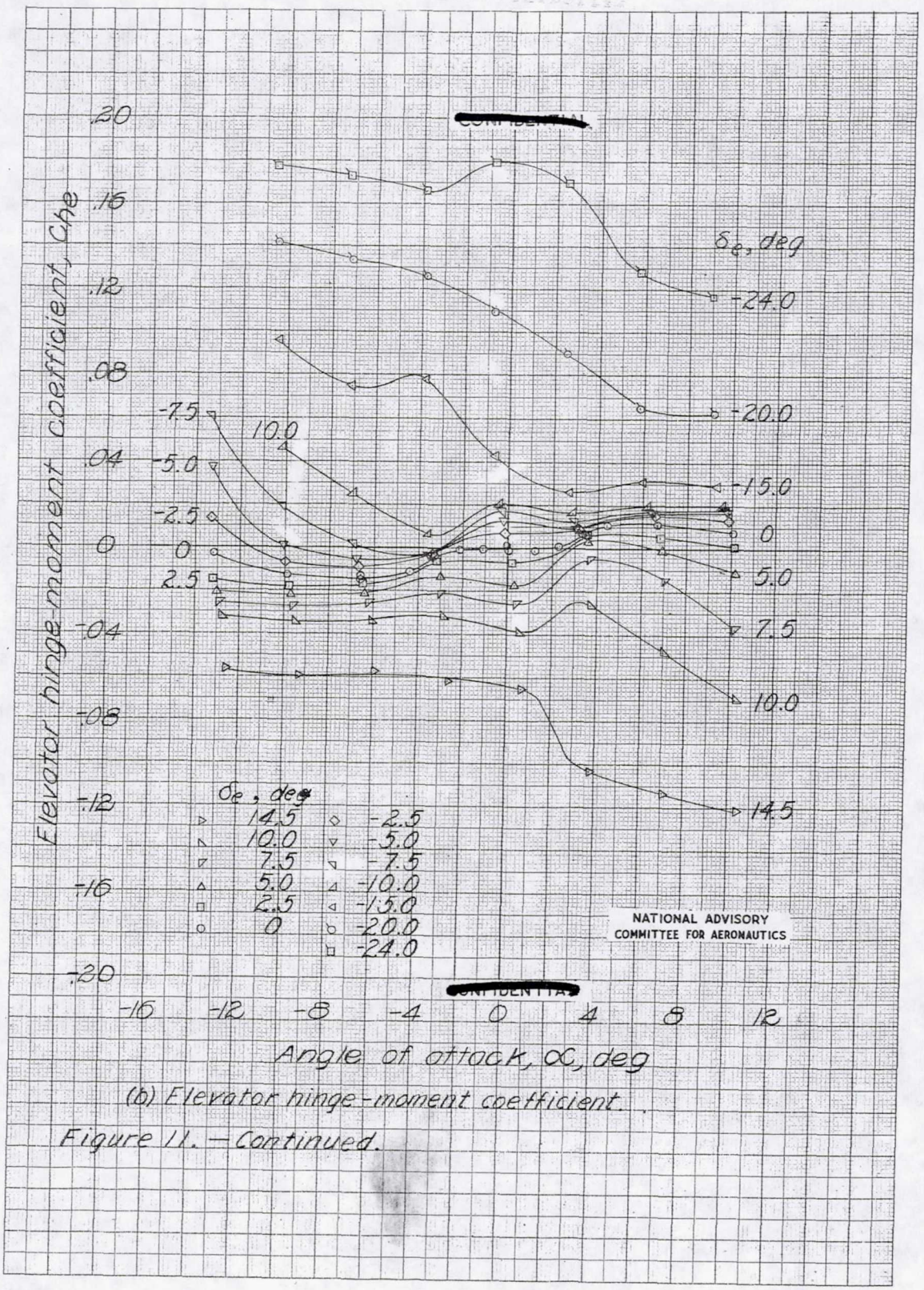

(b) Elevator hinge-moment coefficient.

Figure 11. — Continued.

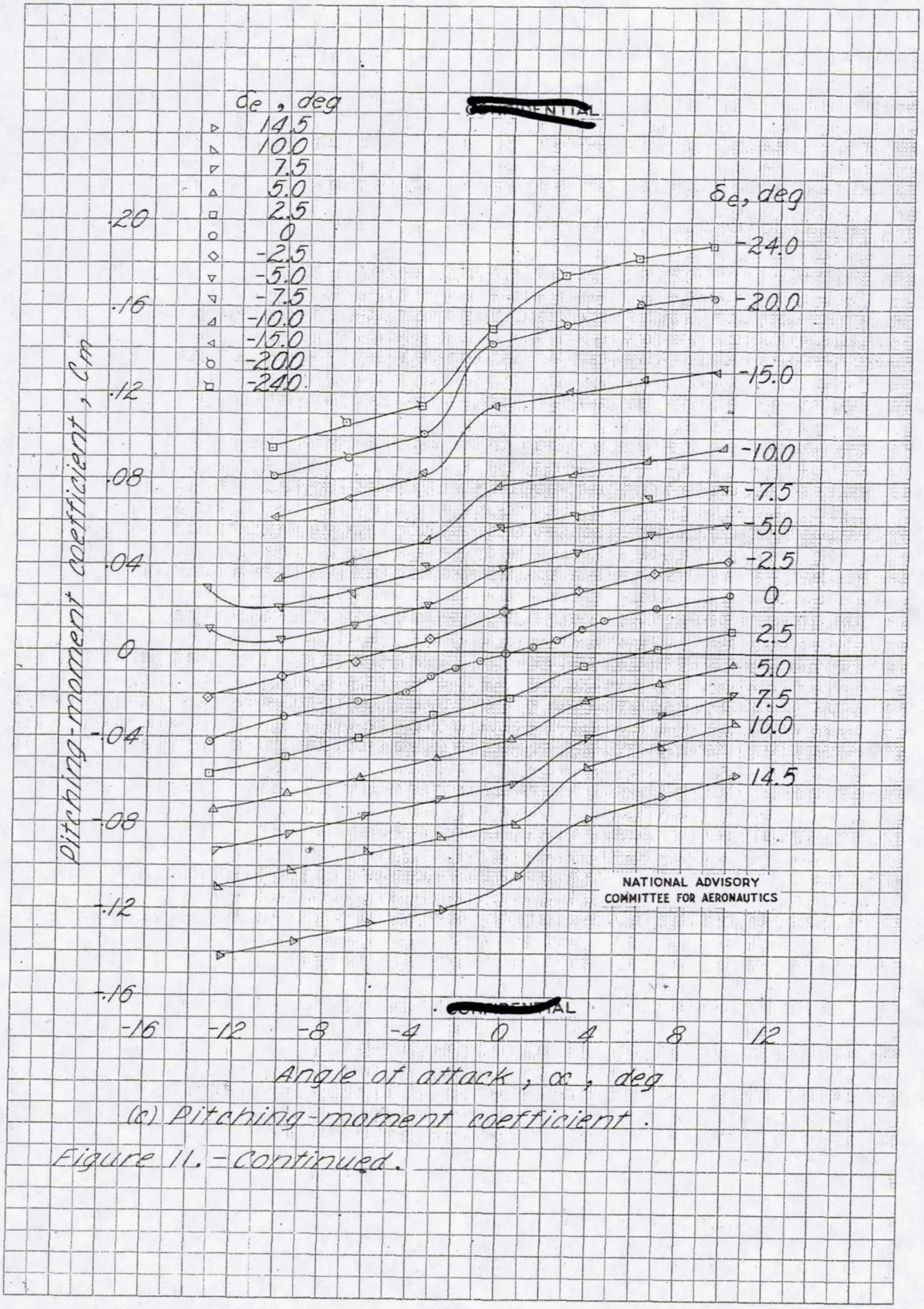

(a) Pitching-moment coefficient.

Figure 11. - Continued.

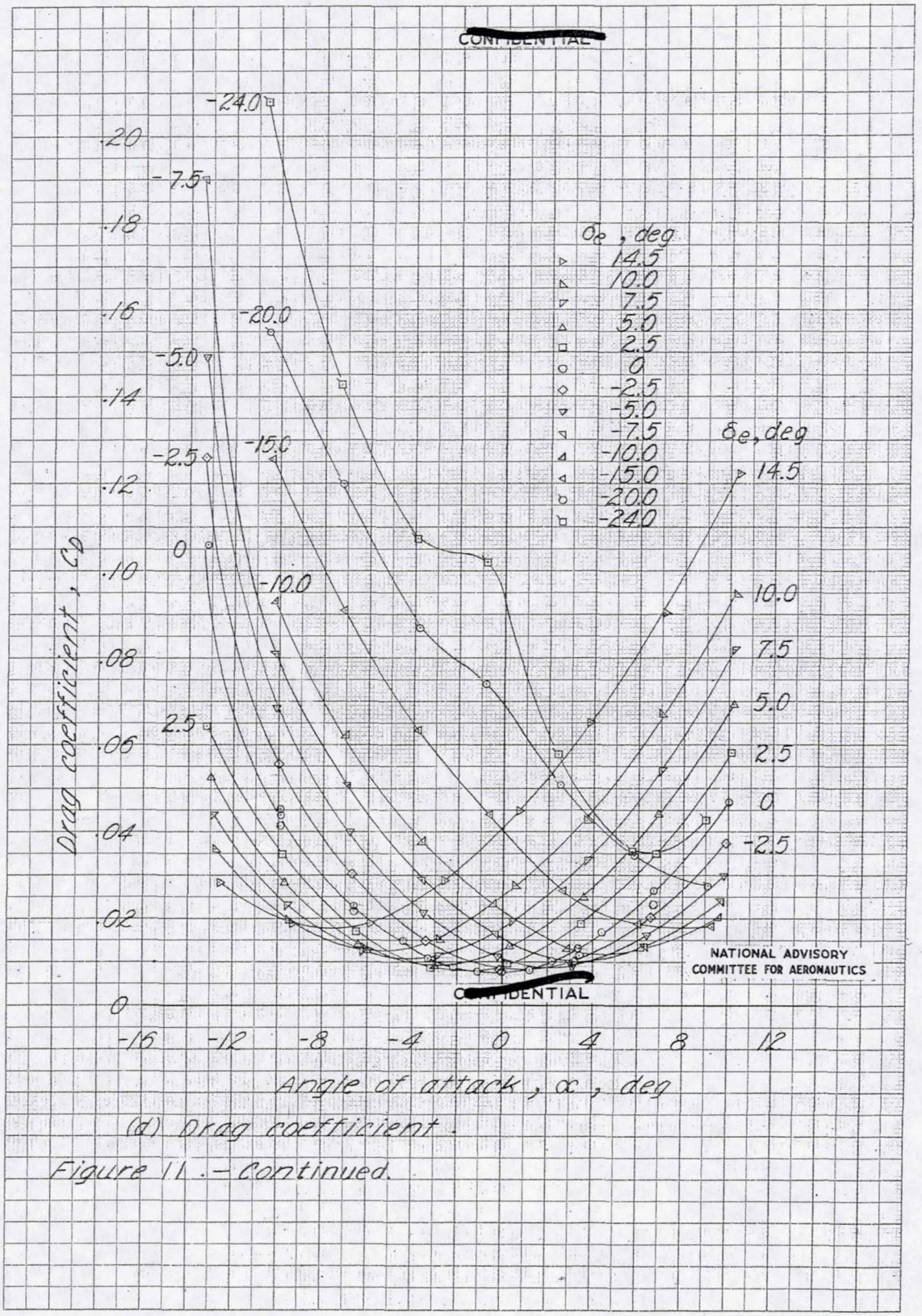

(d) Drag coefficient.

Figure 11.- Continued.

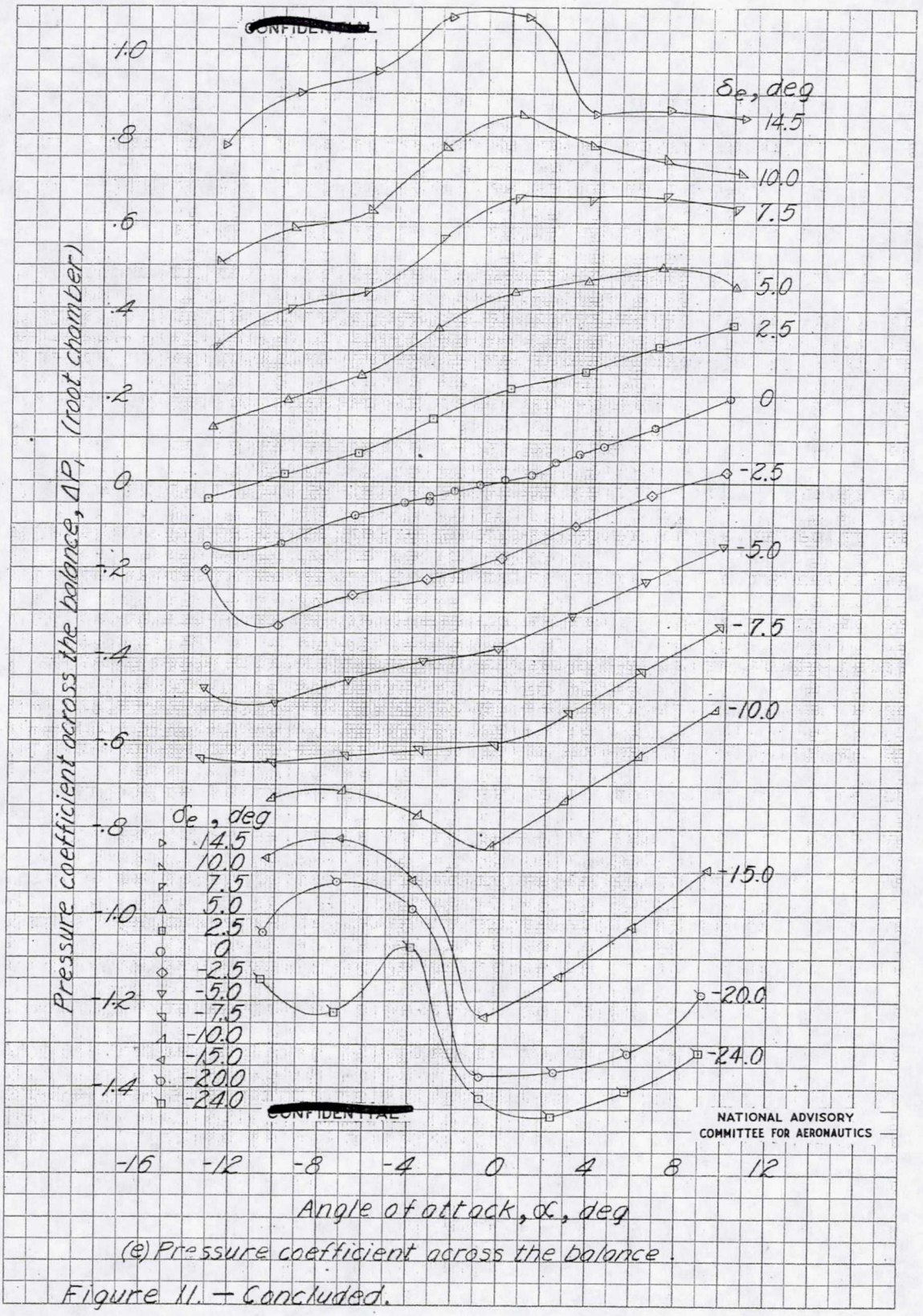

(e) Pressure coefficient across the balance.

Figure 11. — Concluded.

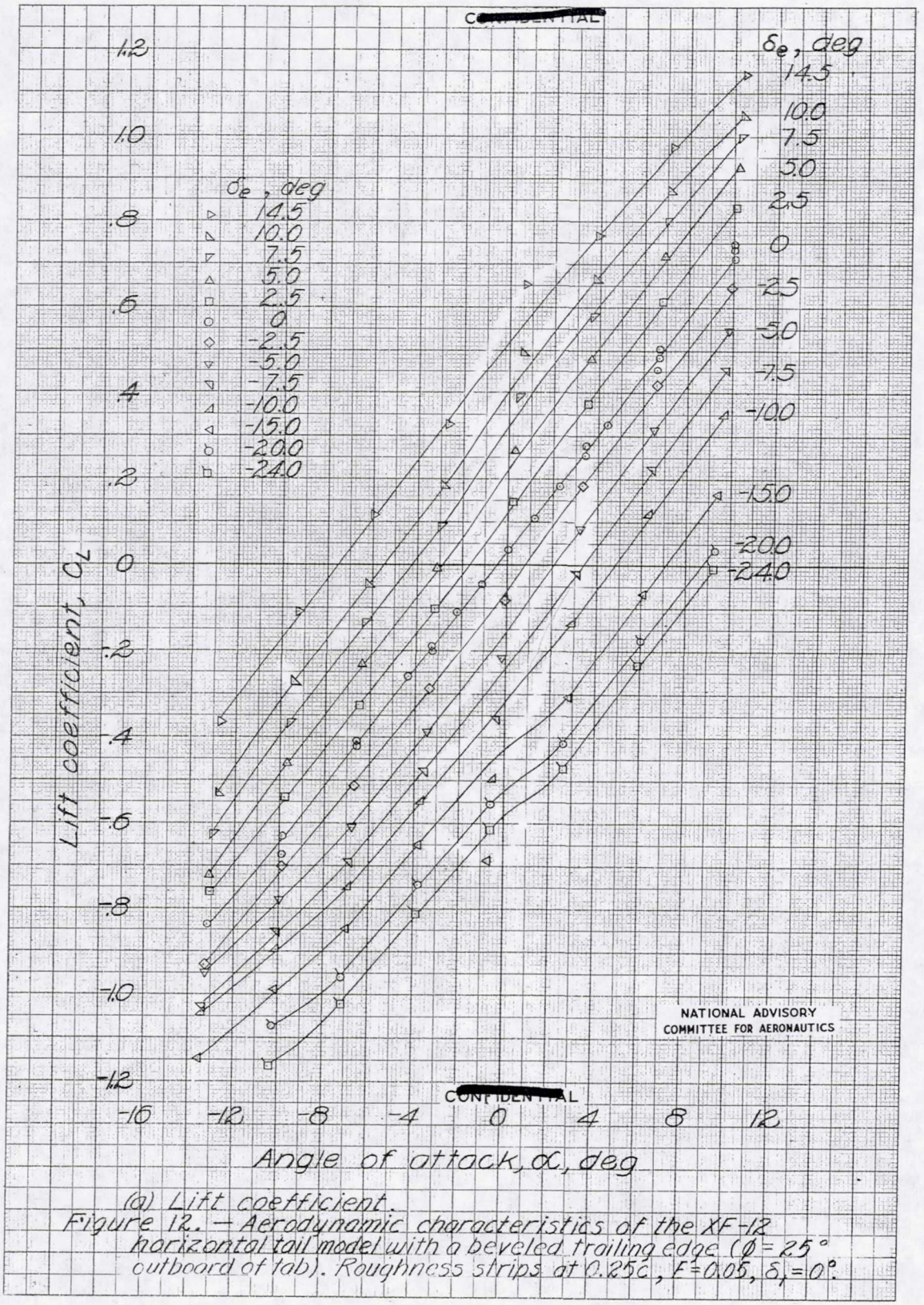

(a) Lift coefficient.

Figure 12. — Aerodynamic characteristics of the XF-12 horizontal tail model with a beveled trailing edge ($\phi = 25°$ outboard of tab). Roughness strips at 0.25c, F = 0.05, $\delta_t = 0°$.

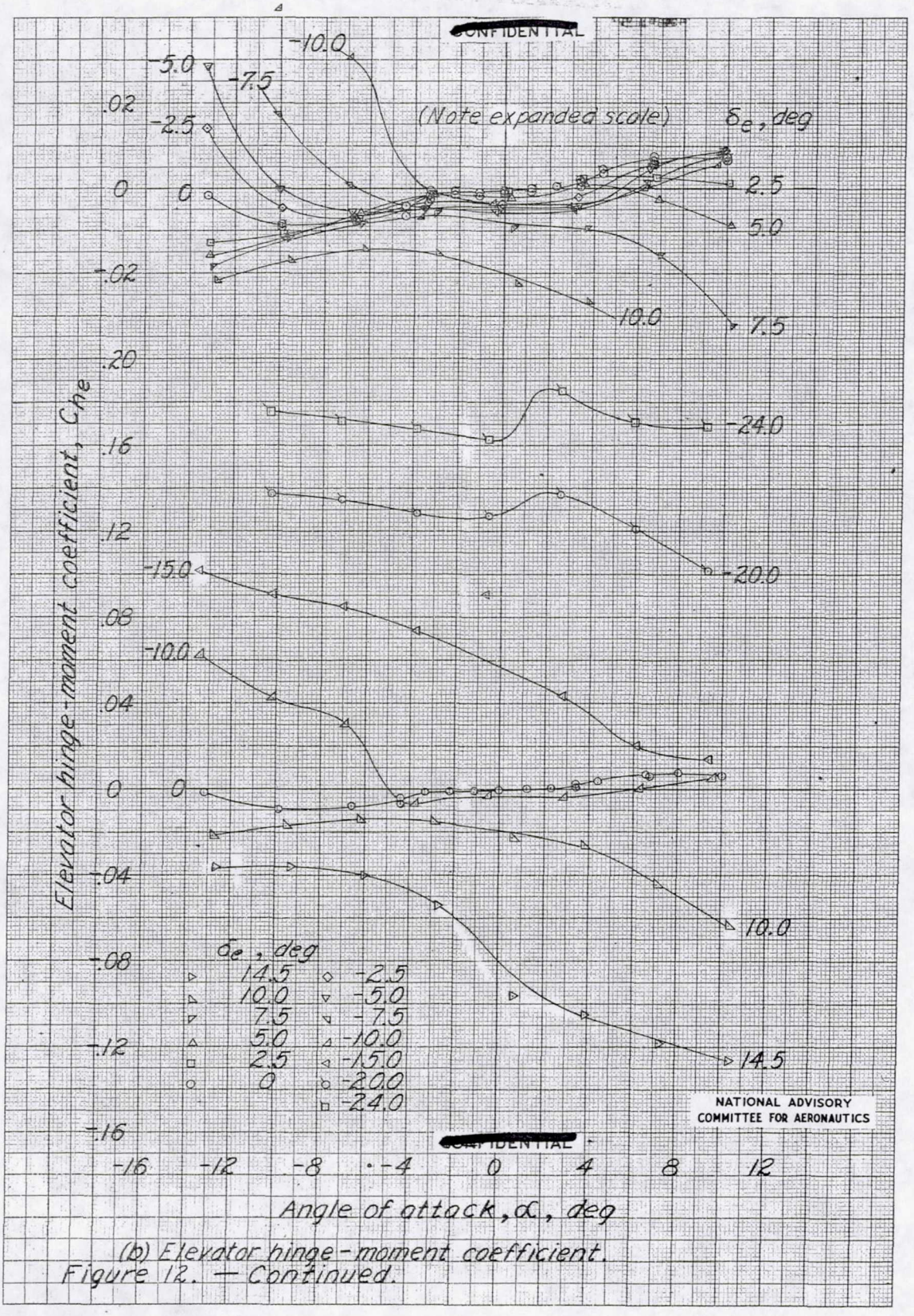

(b) Elevator hinge-moment coefficient.

Figure 12. — Continued.

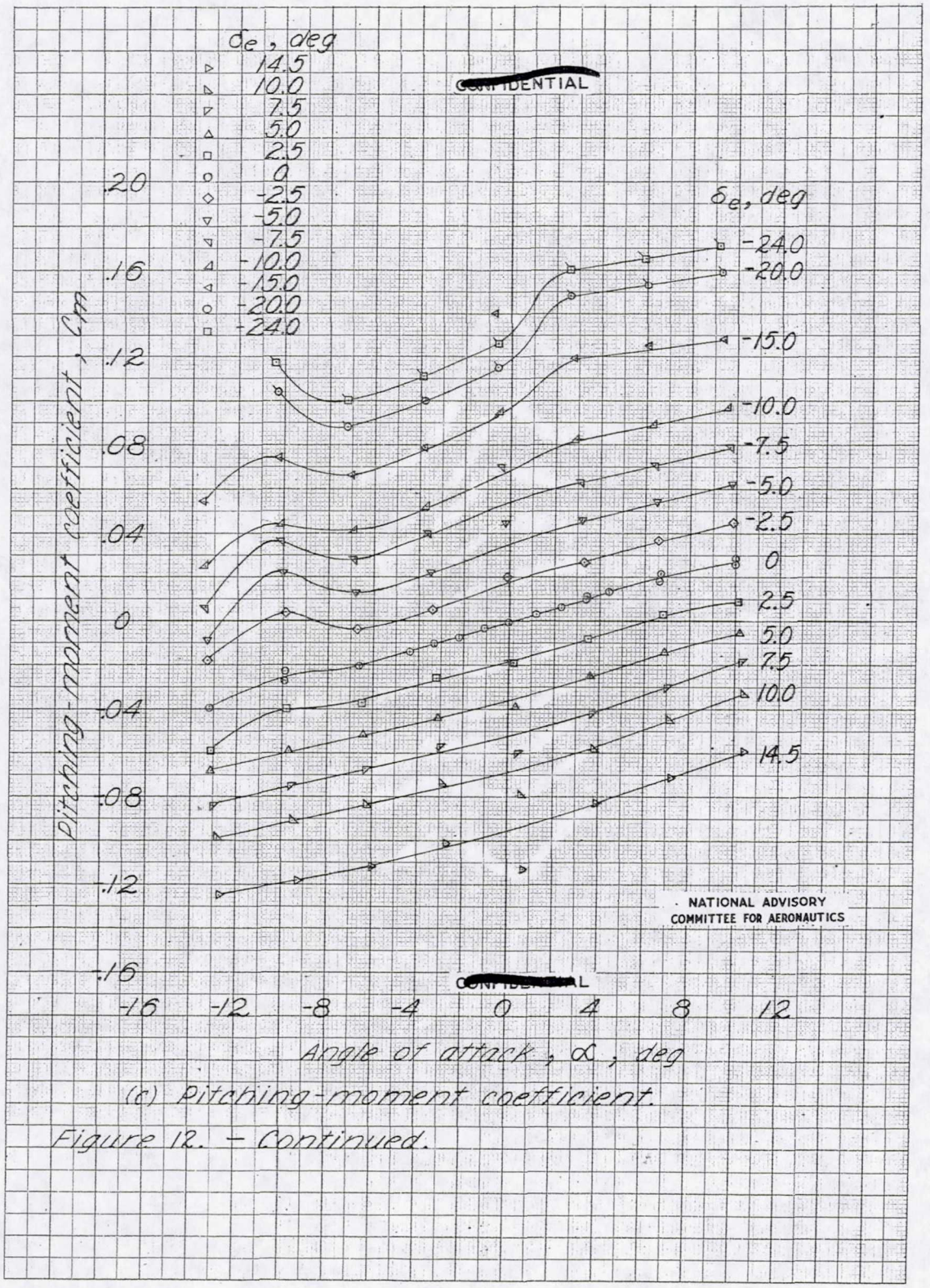

(c) Pitching-moment coefficient.

Figure 12. – Continued.

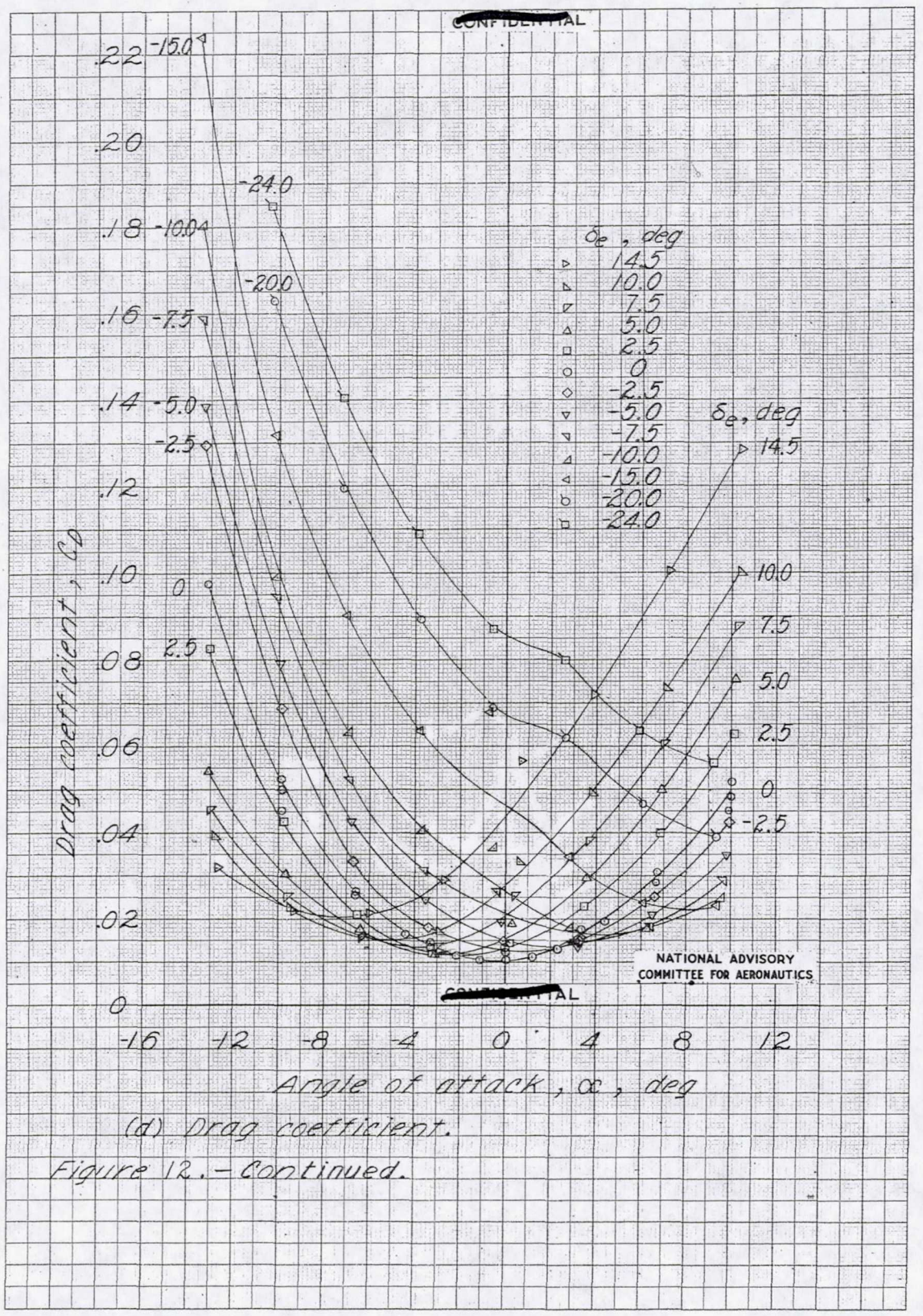

(d) Drag coefficient.

Figure 12.- Continued.

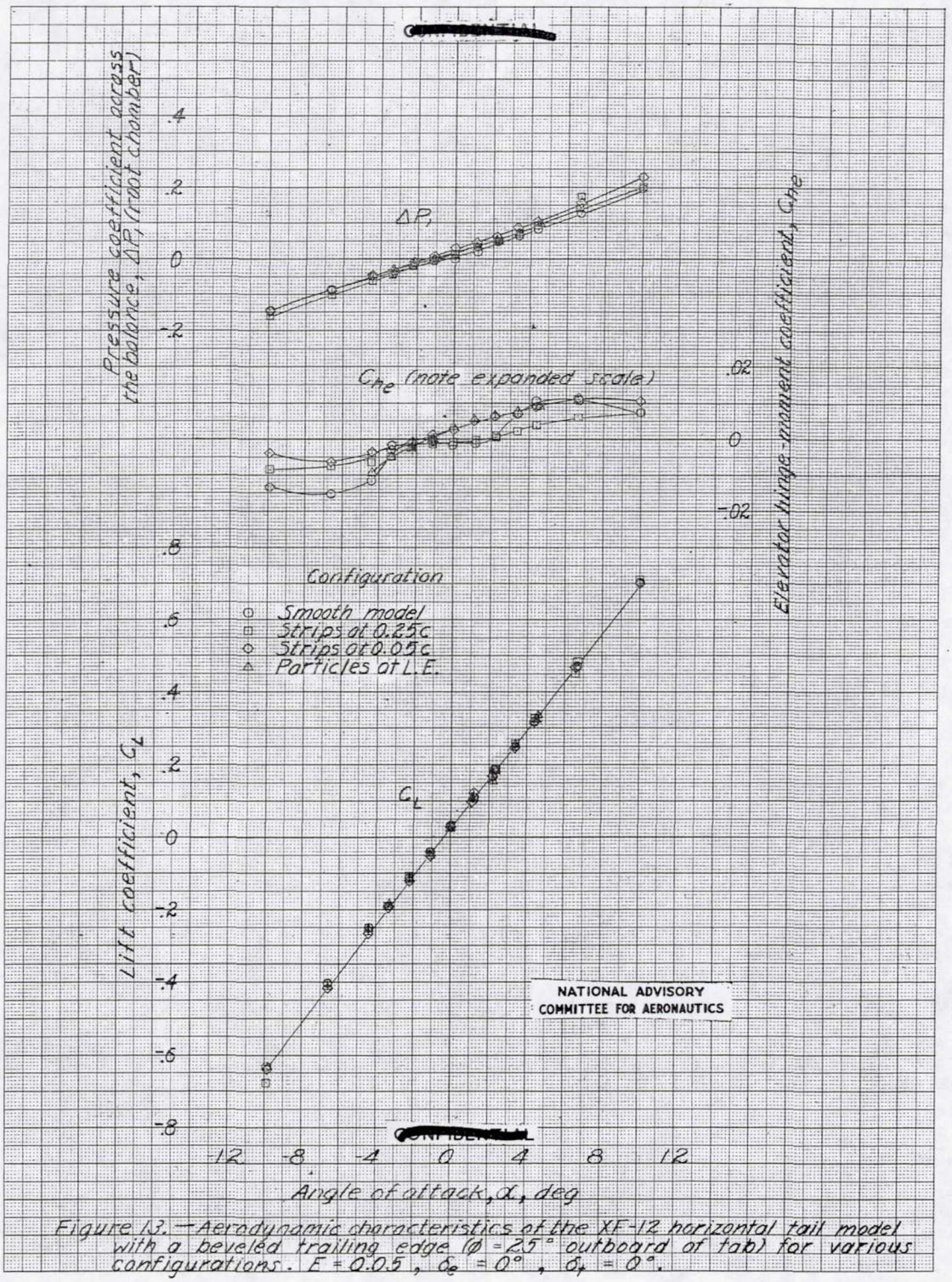

Figure 13.—Aerodynamic characteristics of the XF-12 horizontal tail model with a beveled trailing edge (Ø = 25° outboard of tab) for various configurations. E = 0.05, δ_e = 0°, δ_t = 0°.

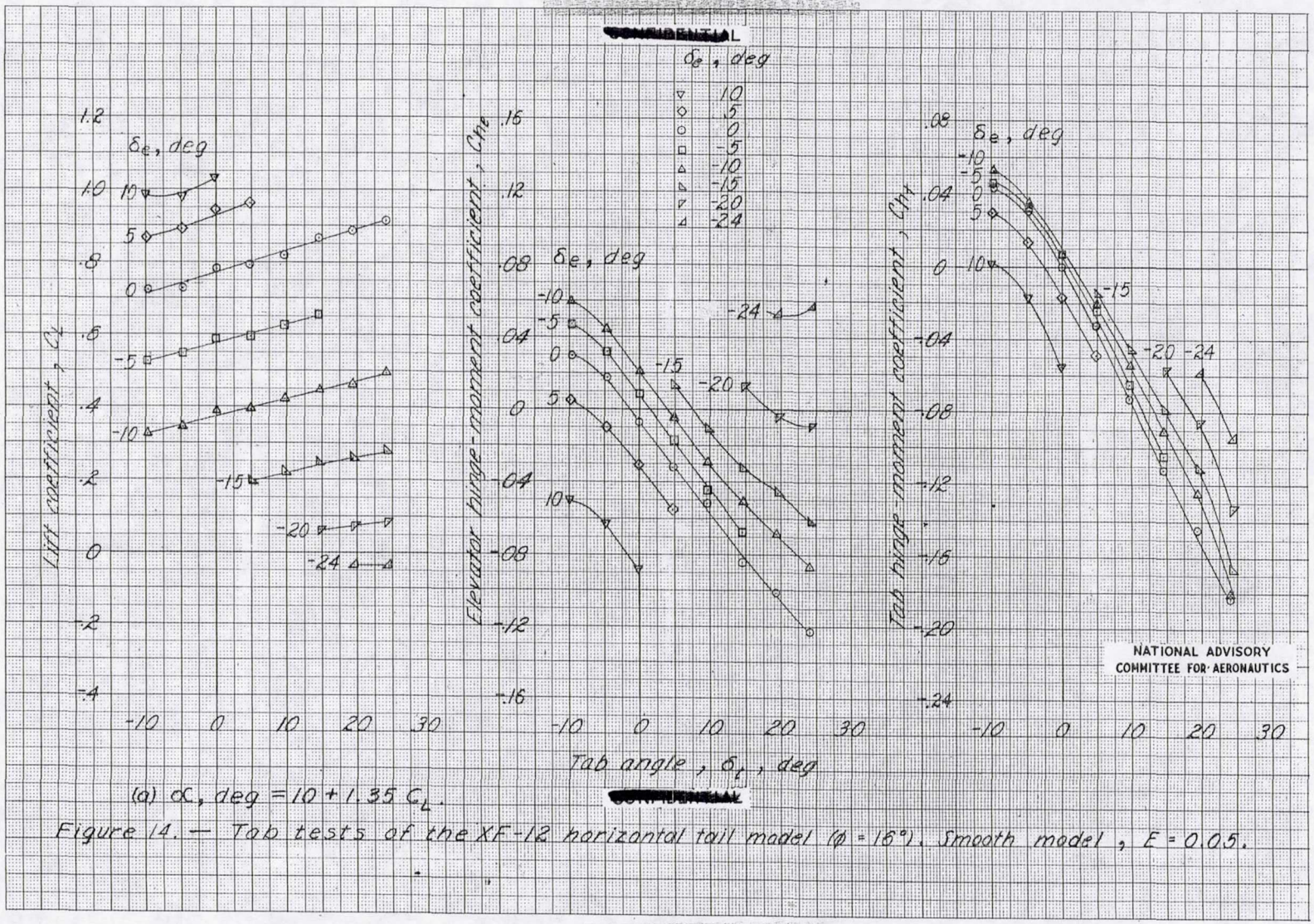

(a) α, deg = 10 + 1.35 C_L.

Figure 14. — Tab tests of the XF-12 horizontal tail model (ϕ = 18°). Smooth model, E = 0.05.

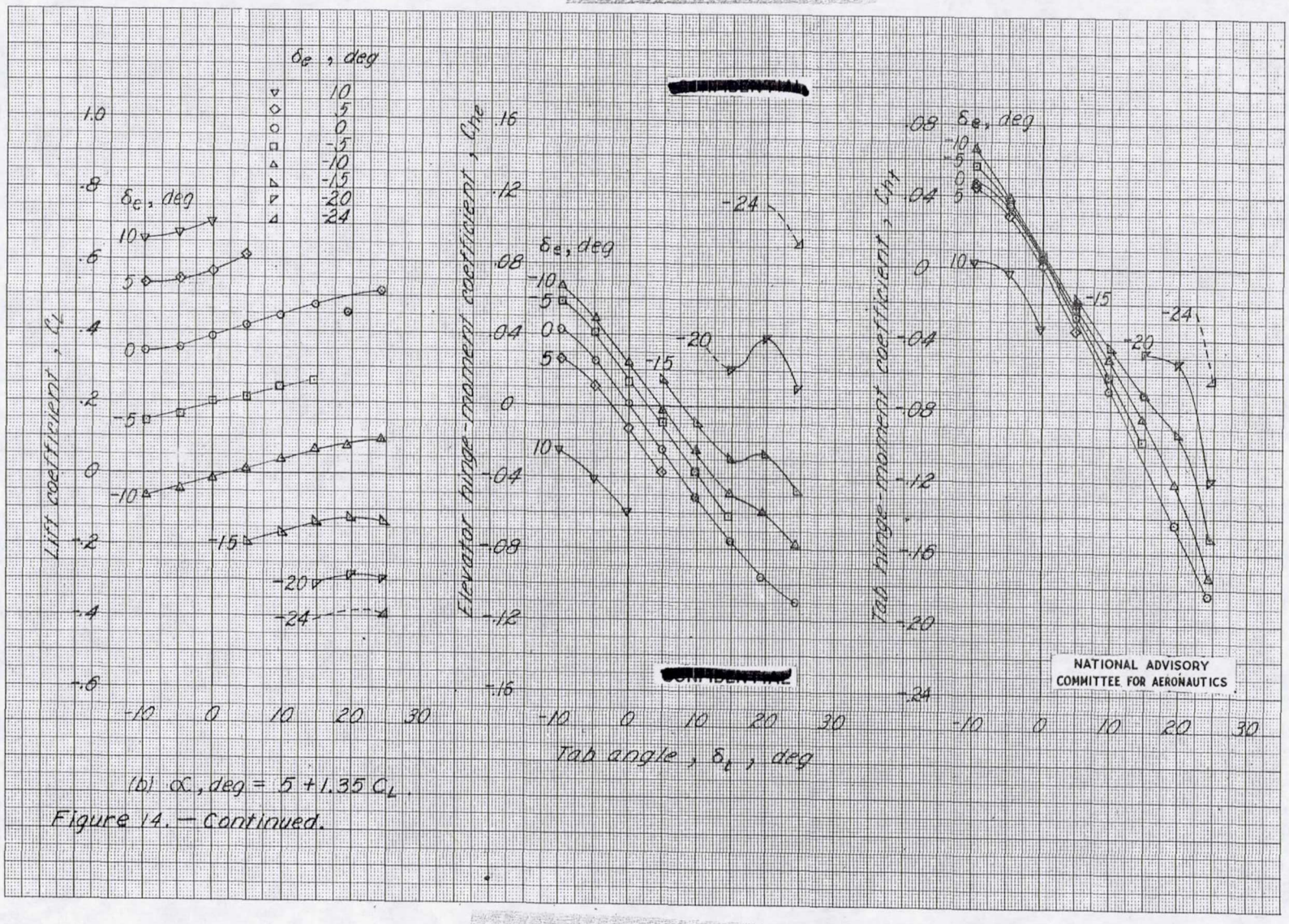

(b) α, deg = 5 + 1.35 C_L.

Figure 14. — Continued.

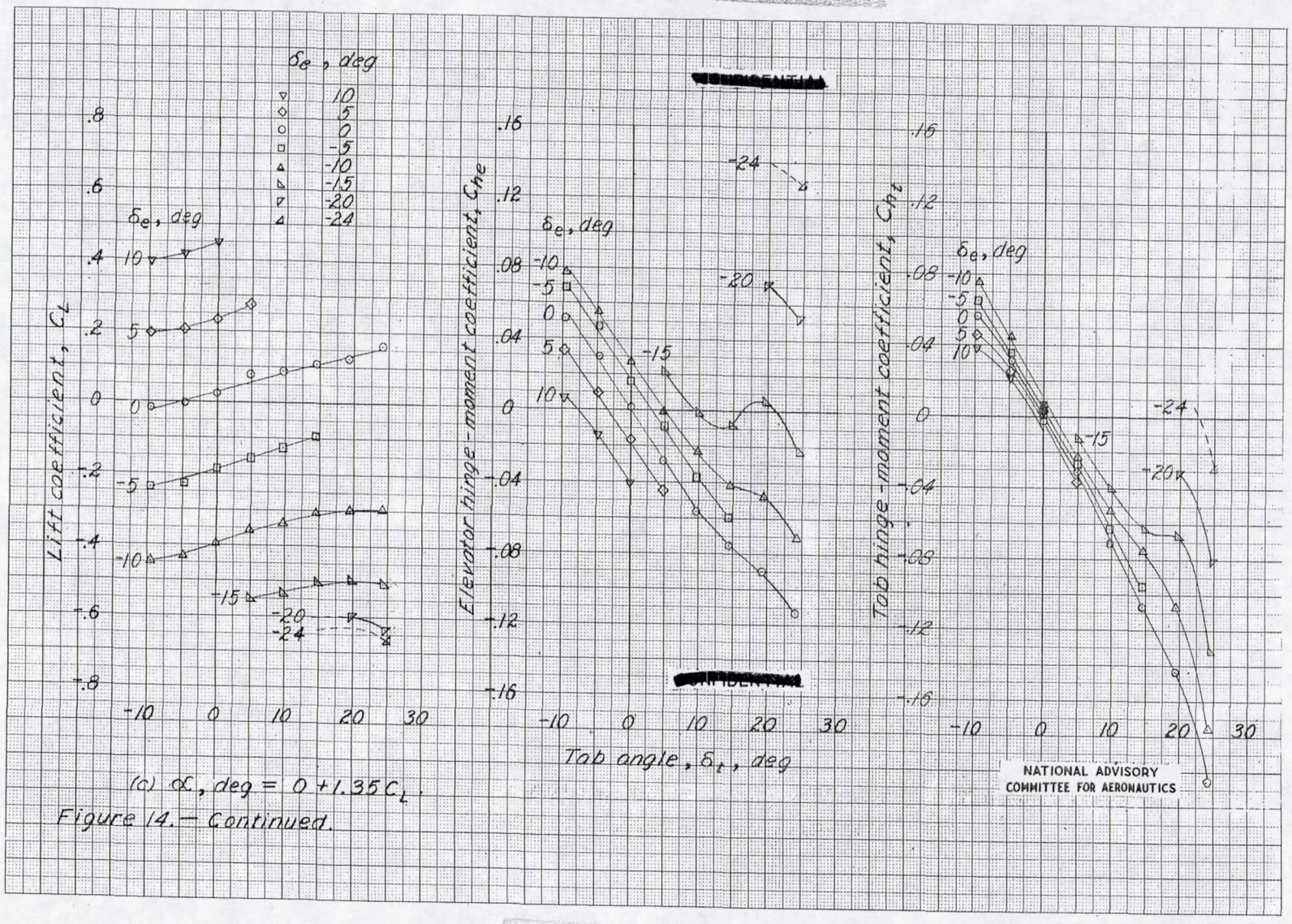

(c) α, deg = 0 + 1.35 C_L.

Figure 14. — Continued.

MR No. L5D12

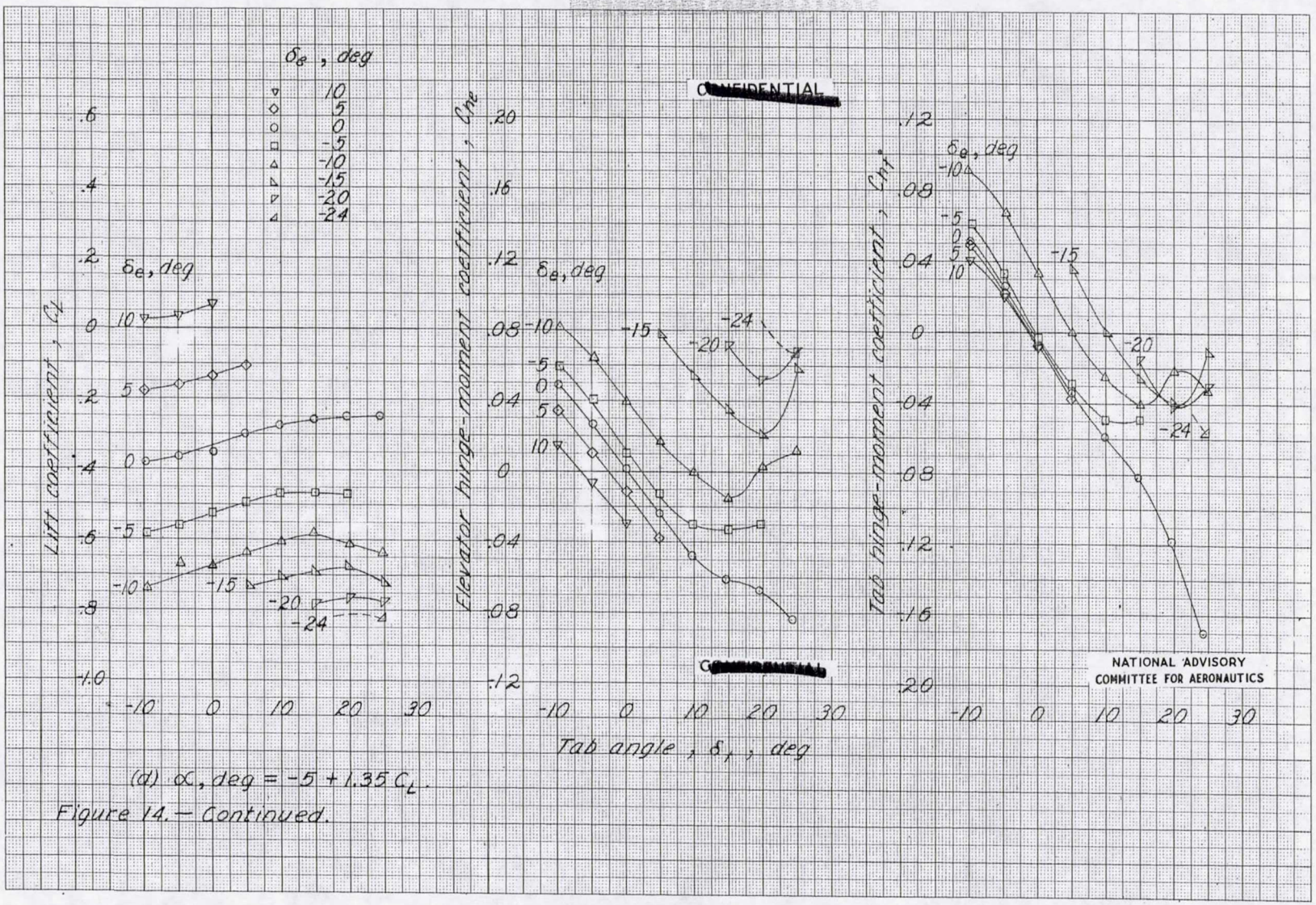

(d) α, deg = $-5 + 1.35\,C_L$.

Figure 14.— Continued.

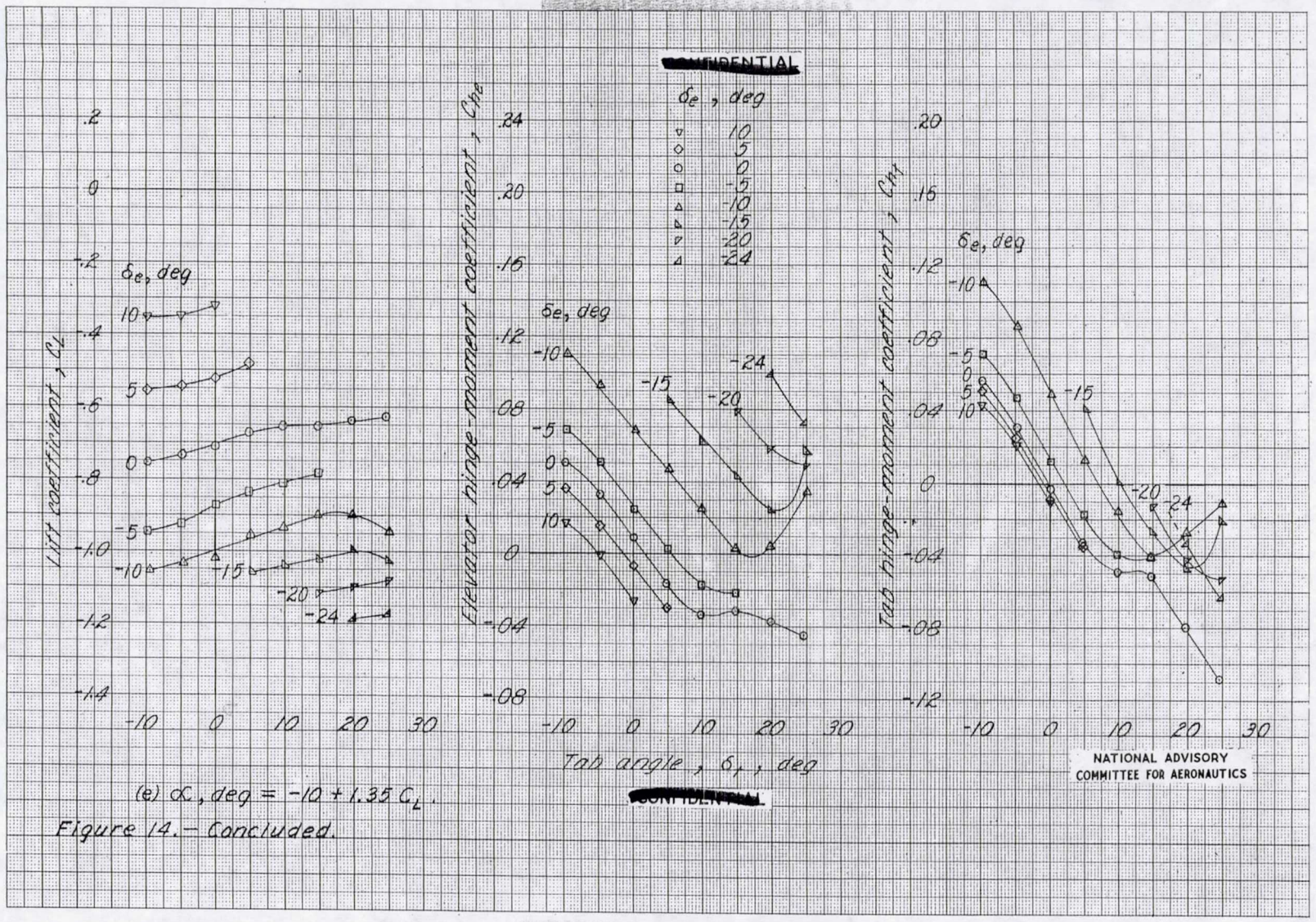

(e) α, deg = $-10 + 1.35\ C_L$.

Figure 14.- Concluded.

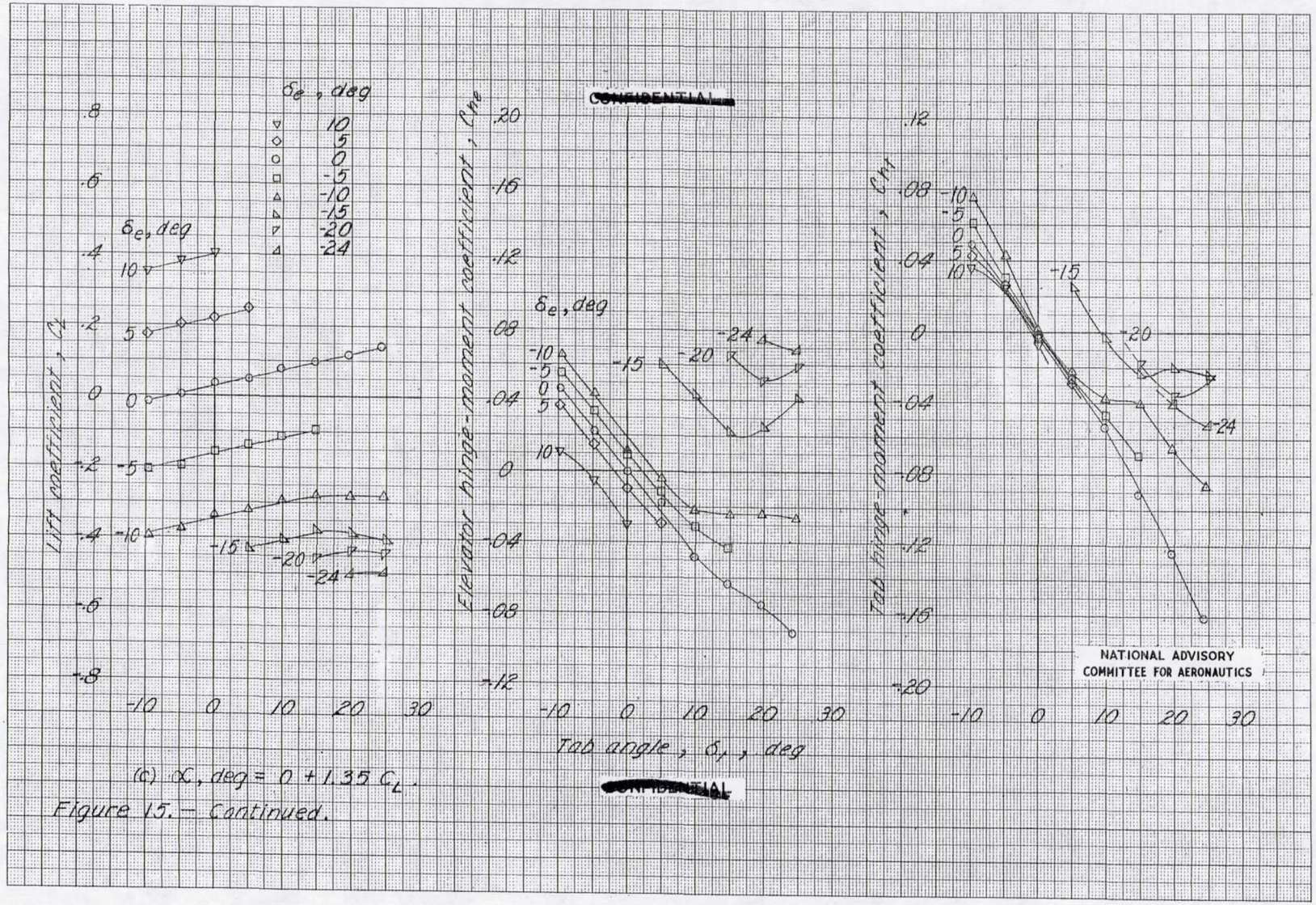

(c) α_t, deg = 0 + 1.35 C_L.

Figure 15.— Continued.

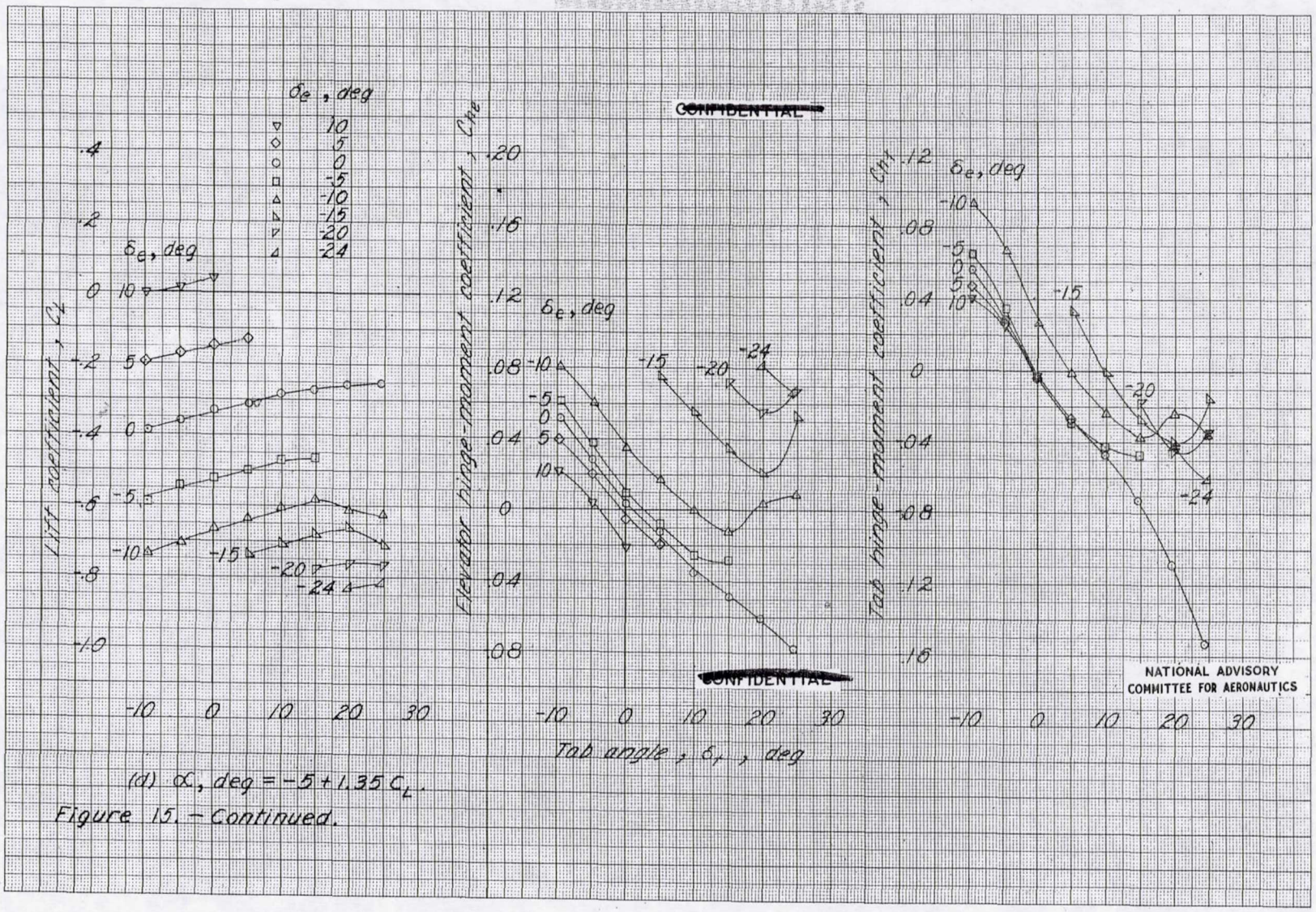

(d) α, deg = $-5 + 1.35\,C_L$.

Figure 15. – Continued.

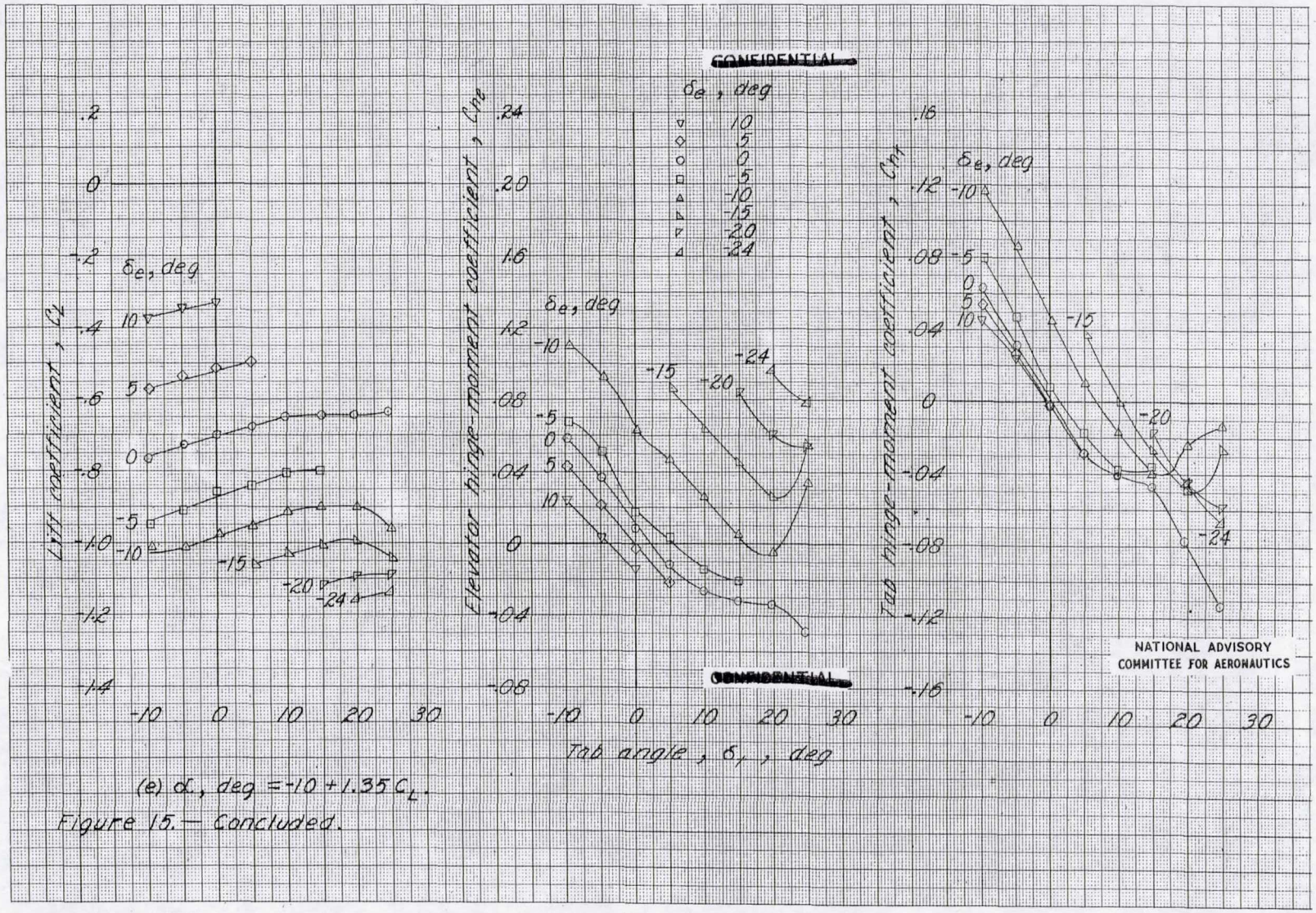

(e) α_t, deg $= -10 + 1.35\,C_L$.

Figure 15.— Concluded.

MR No. L5D12

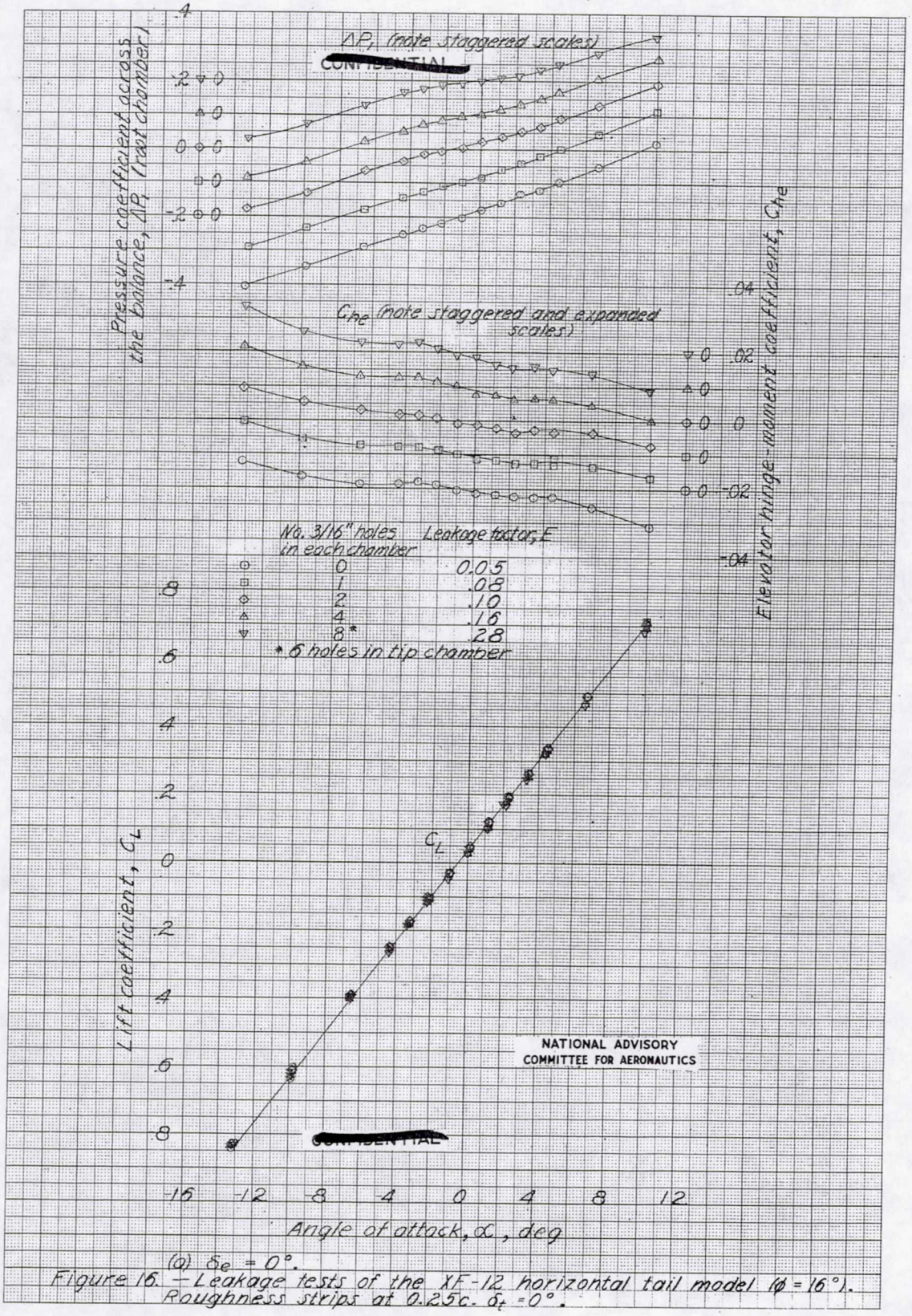

(a) $\delta_e = 0°$.

Figure 16. — Leakage tests of the XF-12 horizontal tail model ($\phi = 16°$). Roughness strips at 0.25c. $\delta_t = 0°$.

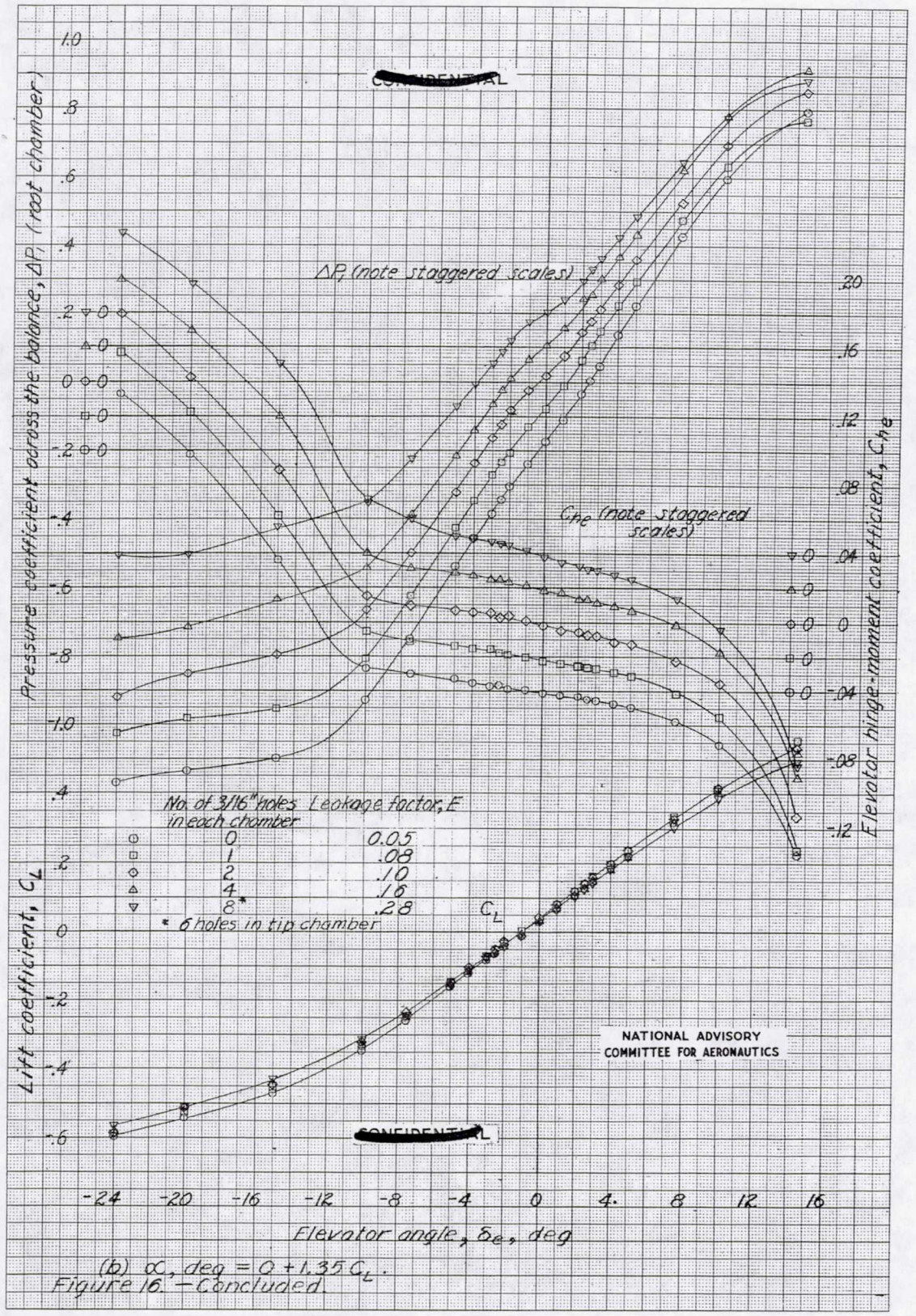

(b) α, deg = 0 + 1.35 C_L.

Figure 16.—Concluded.

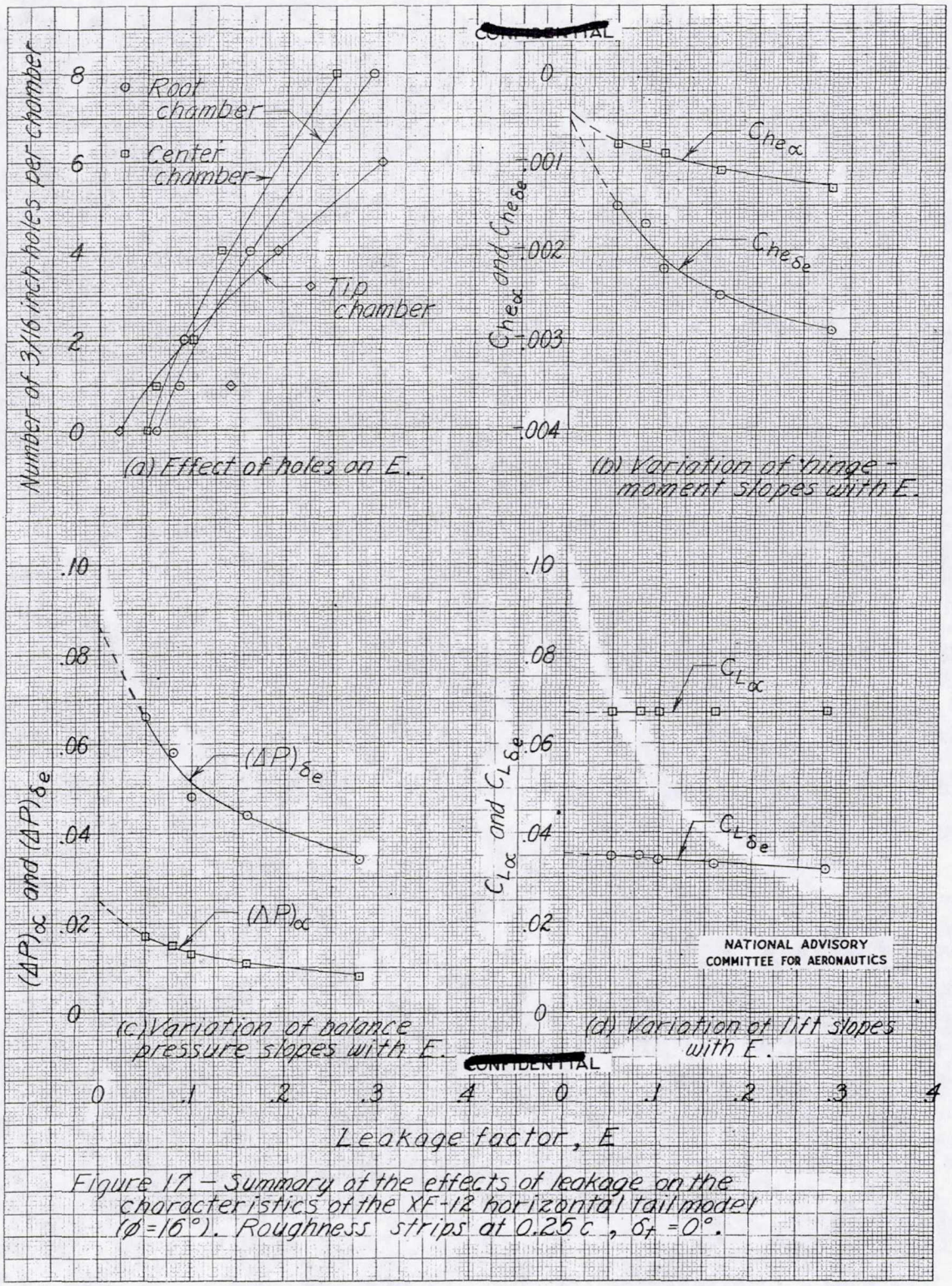

Figure 17 – Summary of the effects of leakage on the characteristics of the XF-12 horizontal tail model ($\phi = 16°$). Roughness strips at 0.25 c, $\delta_f = 0°$.

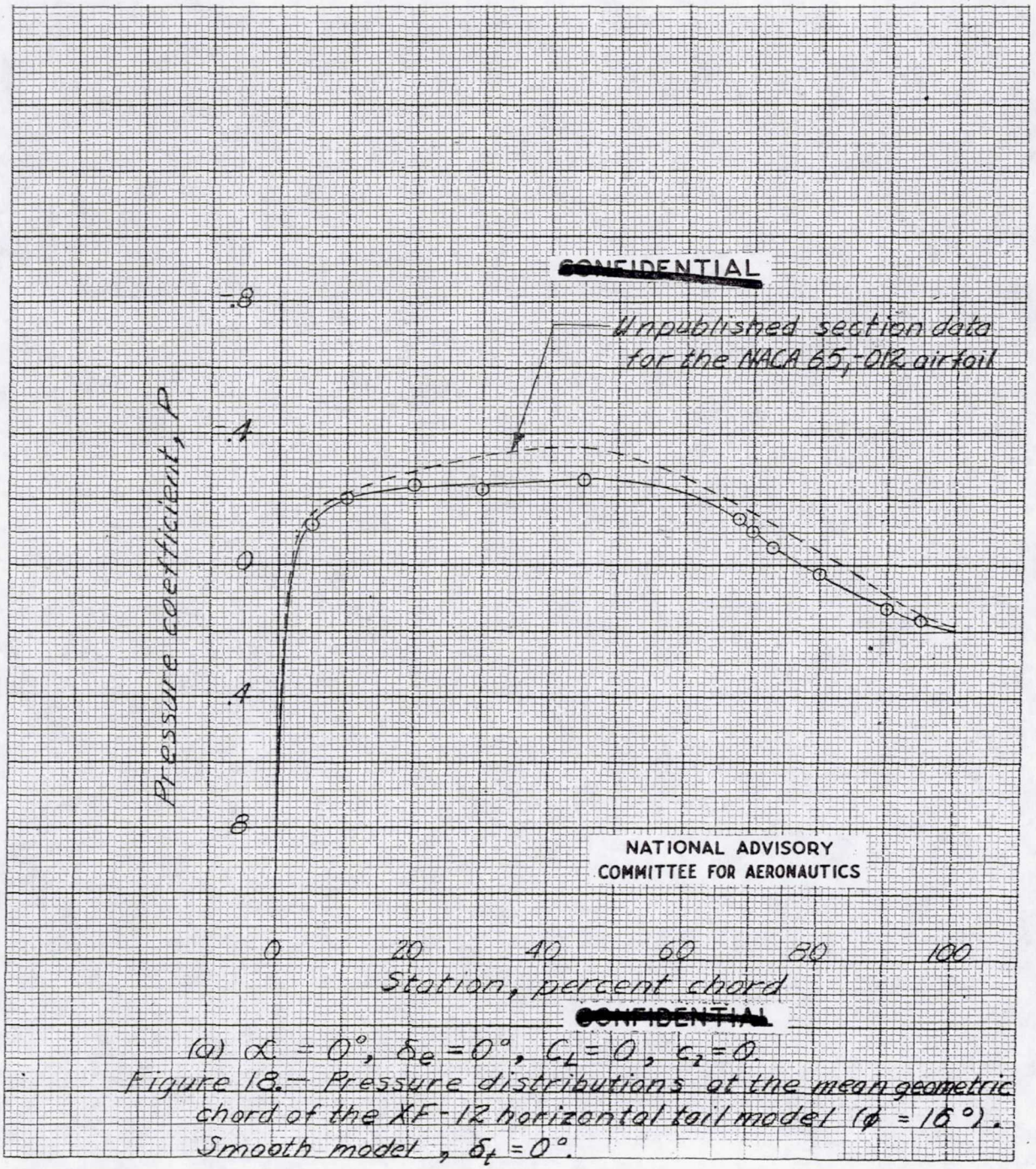

(a) $\alpha = 0°$, $\delta_e = 0°$, $C_L = 0$, $c_t = 0$.

Figure 18.— Pressure distributions at the mean geometric chord of the XF-12 horizontal tail model ($\phi = 16°$). Smooth model, $\delta_t = 0°$.

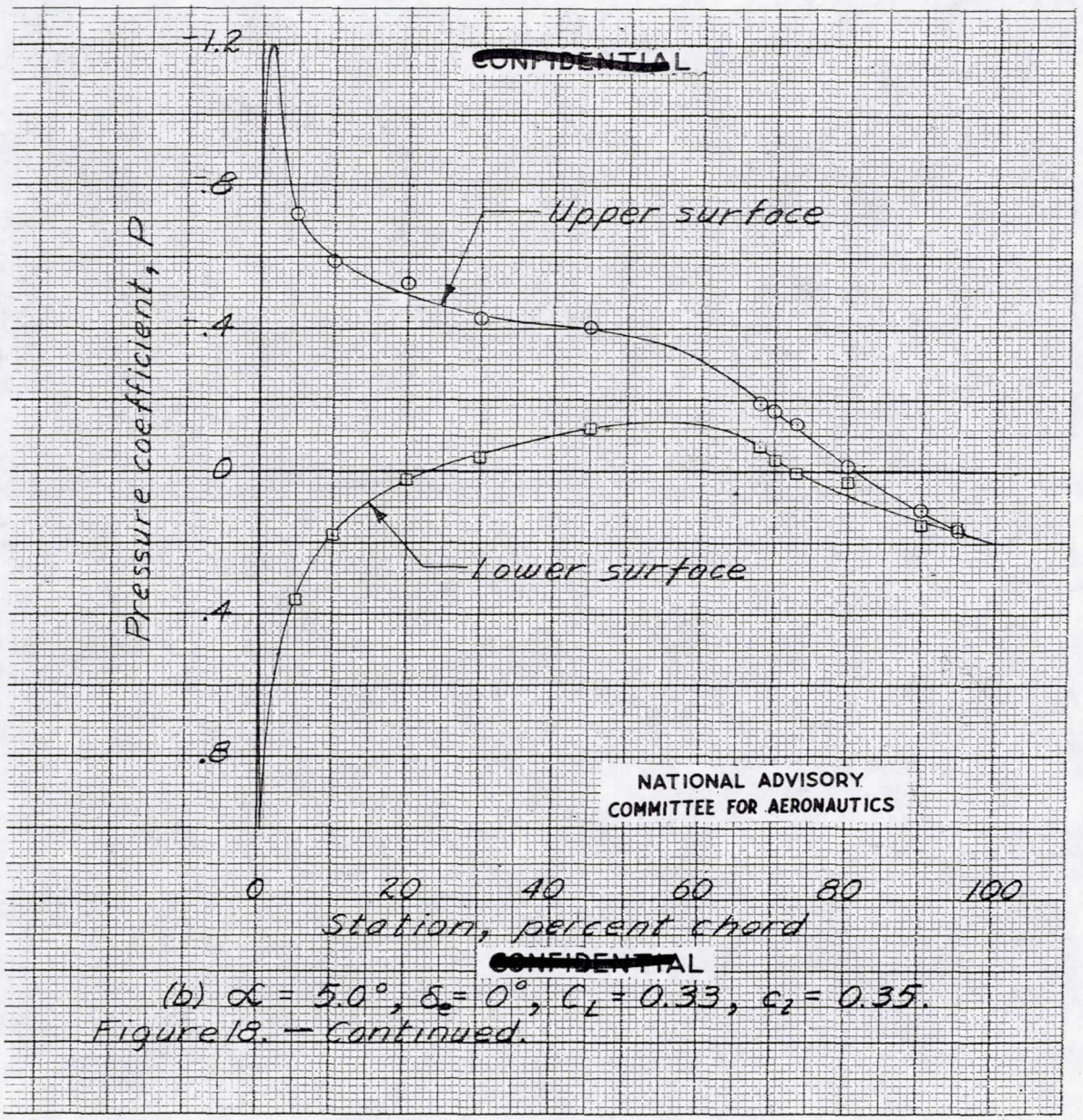

(b) $\alpha = 5.0°$, $\delta_e = 0°$, $C_L = 0.33$, $c_l = 0.35$.

Figure 18. — Continued.

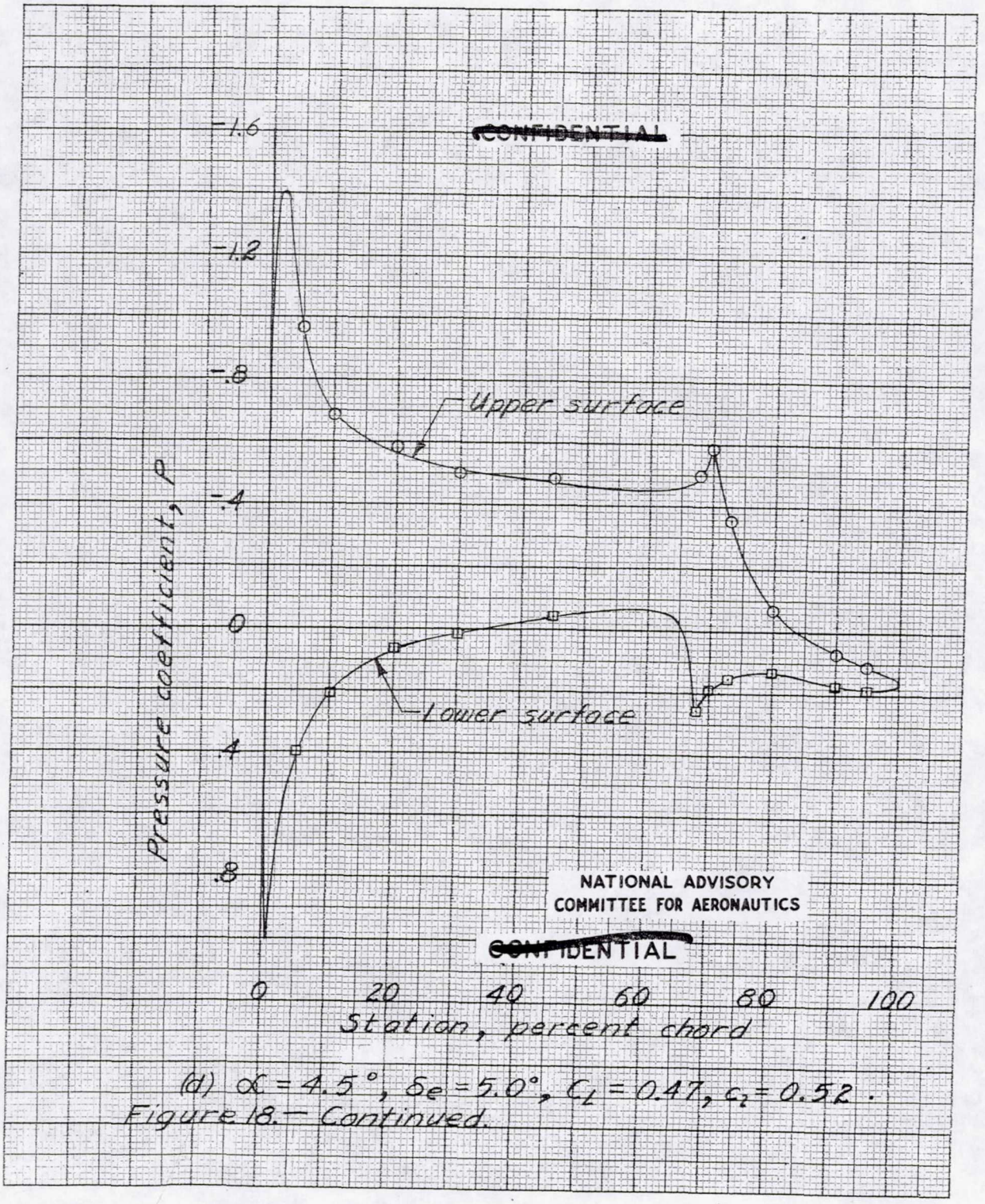

(d) $\alpha = 4.5°$, $\delta_e = 5.0°$, $C_L = 0.47$, $c_z = 0.52$.

Figure 18.— Continued.

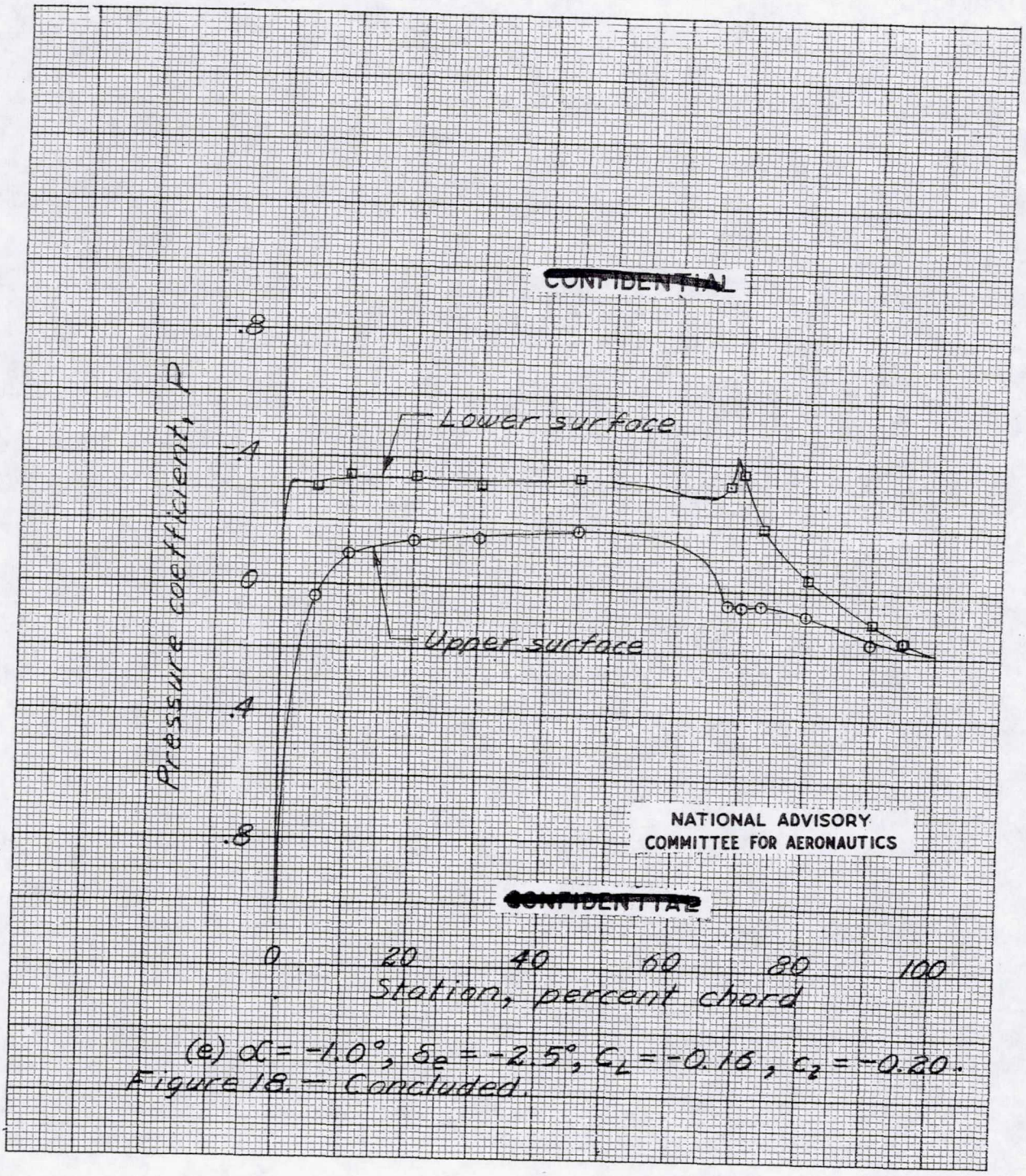

(e) $\alpha = -1.0°$, $\delta_e = -2.5°$, $C_L = -0.16$, $C_z = -0.20$.

Figure 18. — Concluded.

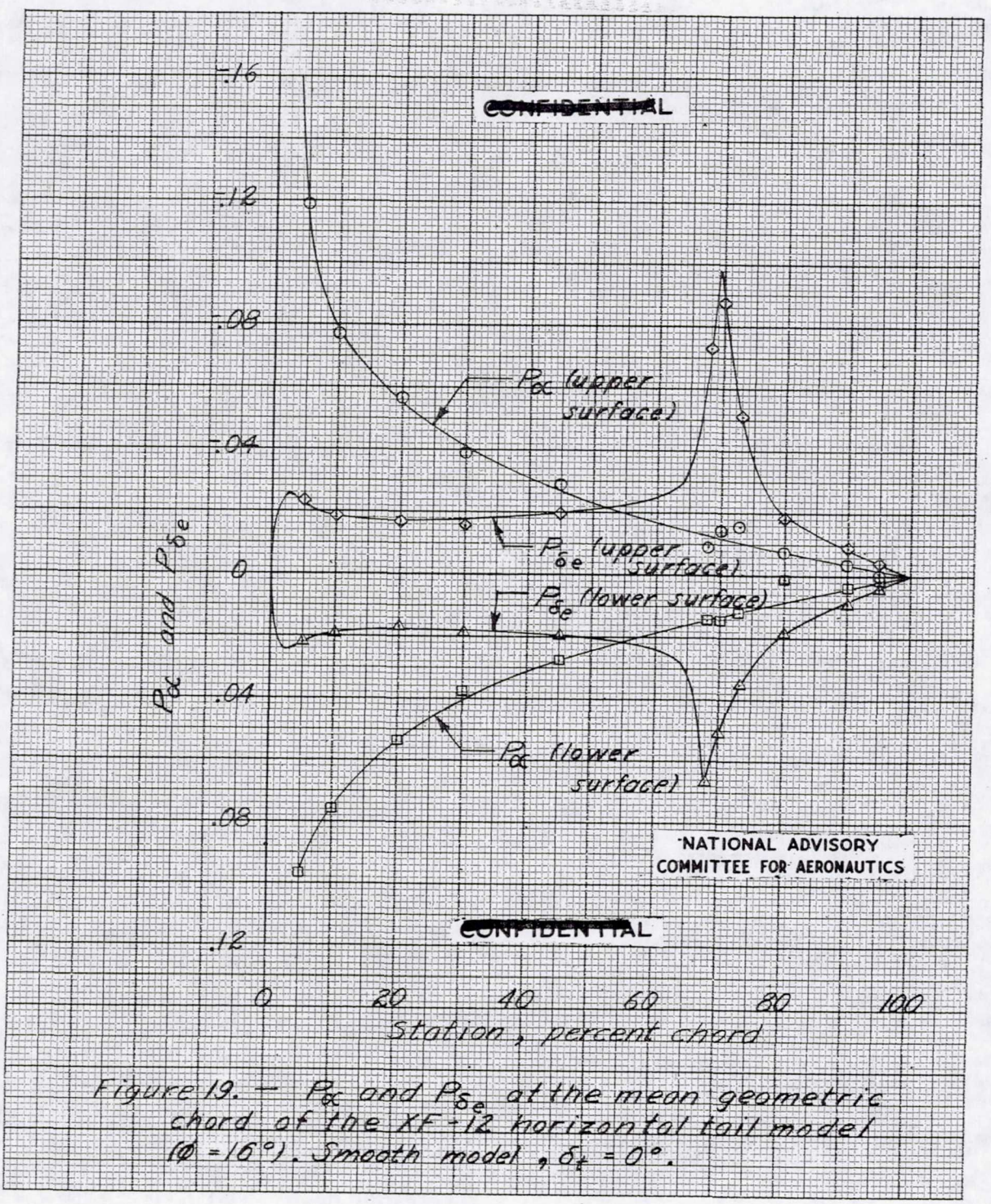

Figure 19. — P_{α} and $P_{\delta e}$ at the mean geometric chord of the XF-12 horizontal tail model ($\phi = 16°$). Smooth model, $\delta_t = 0°$.